ACS OMEGA

http://pubs.acs.org/journal/acsodf

Article

Investigating the Performance of Carboxylate-Alumoxane Nanoparticles as a Novel Chemically Functionalized Inhibitor on Asphaltene Precipitation

Saman Bagherpour, Mohsen Riazi, Masoud Riazi,* Farid B. Cortés,* and Seyed Hamed Mousavi

Cite This: *ACS Omega* 2020, 5, 16149−16164

Read Online

ACCESS | Metrics & More | Article Recommendations | Supporting Information

ABSTRACT: In recent years, researchers have attempted to find some practical approaches for asphaltene adsorption and the prevention or postponement of asphaltene precipitation. Among different techniques, nanotechnology has attracted the researchers' attention to overcome the formation damage resulting from the deposition of asphaltenes. In this study, the application of two types of carboxylate-alumoxane nanoparticles (functionalized boehmite by methoxyacetic acid (BMA) and functionalized pseudo-boehmite by methoxyacetic acid (PBMA)) for asphaltene adsorption and precipitation was investigated. First, the synthesis of two functionalized nanoparticles was performed via the sol−gel method. For the assessment of the adsorption efficiency and adsorption capacity of these nanoparticles toward asphaltene adsorption, the batch adsorption experiments applying ultraviolet−visible (UV−Vis) spectroscopy were performed. The Langmuir and Freundlich isotherms were studied to describe the interaction between asphaltene molecules and carboxylate-alumoxane nanoparticles. For determining the "onset" point of asphaltene precipitation, the indirect method, which was based on the difference in the optical property of various solutions containing different concentrations of asphaltene, was utilized by applying UV−Vis spectroscopy. The isotherm models indicate that the adsorption of asphaltene on the surface of nanoparticles is better fitted to the Freundlich isotherm model compared with the Langmuir model. In the presence of PBMA (0.1 wt %), the onset point was delayed around 26, 20, and 17% in the asphaltene concentrations of 1000, 3000, and 5000 ppm, respectively, in comparison with their reference synthetic oils. On the other hand, these postponements for BMA nanoparticles (0.1 wt %) were 17%, 9%, and insignificant for the asphaltene concentrations of 1000, 3000, and 5000 ppm, respectively. The results reveal that two functionalized nanoparticles tend to adsorb asphaltene molecules and have a positive impact on the postponement of asphaltene precipitation due to molecular interactions between the surface of carboxylate-alumoxane nanoparticles and asphaltene molecules. However, PBMA nanoparticles exhibited better performance on the asphaltene adsorption and postponement of asphaltene precipitation, which is related to its smaller size, as well as higher surface area, compared with BMA nanoparticles.

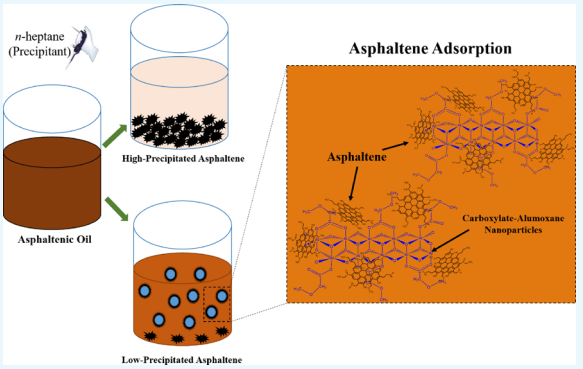

1. INTRODUCTION

Asphaltenes are materials that are commonly found in crude oil, with a propensity to precipitate and deposit in the reservoir pore walls. Changes in pressure, temperature, and composition are the most critical factors that result in asphaltene precipitation.[1,2] Asphaltene molecules represent the most polar and heaviest constituents of crude oil. Six-membered aromatic rings, forming the sizeable graphite-like plate by fusing, construct the chemical structure of most asphaltene molecules.[3] Also, there are numerous alkyl chains in the structure of asphaltene, which indicate that carbon and hydrogen are the significant elements in the asphaltene chemical structure. Moreover, some asphaltene molecules have heteroatoms, such as nitrogen, oxygen, and sulfur, which are the most important elements in their structures. With the asphaltene deposition in the porous media of oil reservoirs, some drawbacks ascribed to the operational problems occur. Stopping the oil production based on the formation damage and increasing the pressure drop, as well as the deposited asphaltene attaching to the tube walls in the transportation stage, are the most critical problems of asphaltene precipitation.[4] Moreover, another important disadvantage is that the catalysts employed in the refining stages will be deactivated by the asphaltene deposition in the refinery vessels.[5]

Received: April 15, 2020
Accepted: June 10, 2020
Published: June 23, 2020

https://dx.doi.org/10.1021/acsomega.0c01732
ACS Omega 2020, 5, 16149−16164

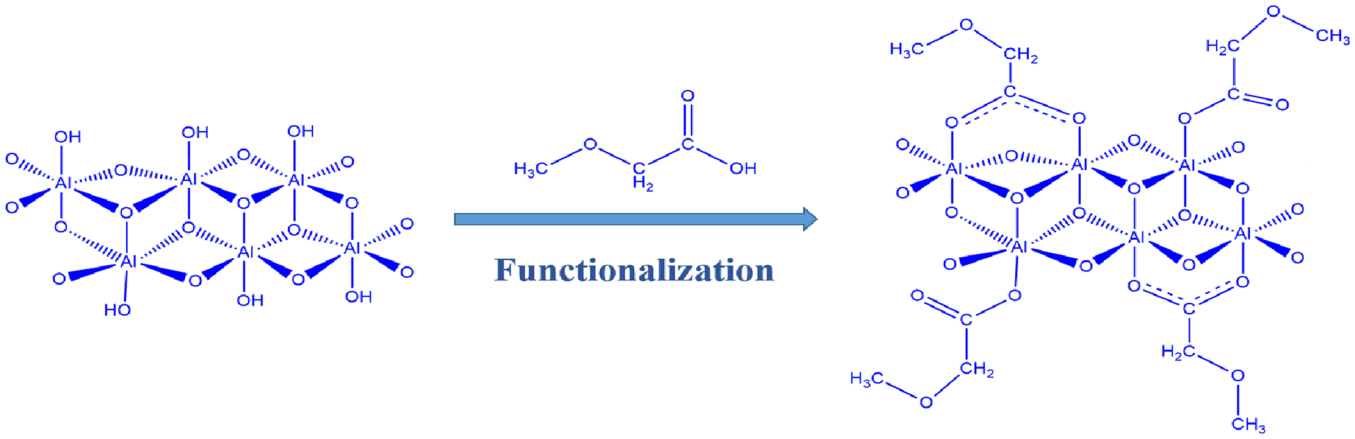

Figure 1. Molecular structure of carboxylate-alumoxane nanoparticles.

To investigate the practical approaches for preventing or postponing the asphaltene precipitation, many researchers endeavor to find practical, cost-effective, and environmentally benign solutions to overcome the asphaltene deposition problems.[6−18] Hu et al.[19] investigated the effect of the ionic liquids based on $[Cnpy]^+$ and $[C_4iql]^+$ cations and the alkylbenzene-derived amphiphiles Cnphol, Cnbsa, and CnbsNa on the asphaltene precipitation. Their proposed mechanism illustrated that due to having high-charge-density anions, ionic liquids could act as effective inhibitors via the destruction of asphaltene associations. León et al.[20] also studied the impact of nonylphenol, native resin, and nonylphenol resin on the inhibition of asphaltene precipitation. To this end, they assessed the adsorption behavior of these chemical materials. They concluded that the effect of nonylphenol resin and native resin is greater than that of nonylphenol due to the penetration of the resins in the micropores of asphaltene, which contributes to the partial breakdown of asphaltene macrostructures. In addition, Dehaghani and Badizad[21] investigated the inhibitory performance of some commercial chemicals for detecting the "onset" point of asphaltene precipitation via a viscometry method. They revealed that the linear dodecyl-benzene sulfonic acid (DBSA) is the best choice for the inhibition of asphaltene deposition due to its inhibitory potentiality, commercial availability, and, more importantly, environmentally benign impacts. They also realized that the amphiphilic attachment on the surface of asphaltene is an equilibrium reaction, which is consistent with the concentration of additive.

Recently, nanotechnology has drawn the researchers' attention as a novel method to tackle the asphaltene precipitation problems.[22−29] Due to appealing characteristics such as small size, high specific surface area, appreciable dispersibility in liquid media, and high adsorption capacity, the utilization of nanoparticles can be considered as an effective method for inhibiting the asphaltene aggregation.[30,31] Nassar et al.[32] studied the impact of the acidic−basic characteristics of alumina nanoparticles on asphaltene adsorption. By investigating these characteristics, they realized that the acidic, basic, and neutral alumina nanoparticles exhibit a definite tendency for asphaltene adsorption. However, the acidic alumina exhibited the most adsorption, resulting from the stronger interactions with the asphaltene structures, and the neutral alumina had the least adsorption value. Moreover, Lu et al.[33] studied the impact of alumina nanoparticles on asphaltene precipitation throughout CO_2 flooding. They stated that the interactions among nanoparticles containing asphaltene are weaker than those among nanoparticles without asphaltene. Consequently, the asphaltenes adsorbed on the nanoparticles remain in a stable condition, causing the inhibition of asphaltene precipitation. More recently, our research group has evaluated several metallic oxides (SiO_2, Al_2O_3, MgO, Fe_2O_3, Fe_3O_4, and these materials with a modified surface), which have been investigated in adsorption tests, aggregation of asphaltenes, and coreflooding tests at reservoir conditions.[34] Surface modification of alumina and silicon dioxide with nickel oxide nanoparticles has shown the best results at a laboratory scale, formulating oil-based nanofluids with a concentration between 300 and 1000 ppm, which have been posteriorly evaluated in field tests.[35] It is worth mentioning that the nanofluids, which resulted in successful inhibition of the precipitation/deposition of asphaltenes based on the adsorption of the asphaltenes and the reduction of its aggregate size, showed an increase in the production and a reduction in the declination rate. In addition, the perdurability of the treatment in the field was up to 18 months.[35] However, the concentrations of nanoparticles and their high energy density in these applications favor their aggregation, which can generate formation damage mainly for some tight and shale reservoirs due to their low and ultralow permeability.

In this research, the asphaltene adsorption and the inhibitory effect of carboxylate-alumoxane nanoparticles on asphaltene precipitation have been investigated. For preparing carboxylate-alumoxane nanoparticles, boehmite and pseudo-boehmite were functionalized with the acidic method (Figure 1) and are called BMA and PBMA, respectively. Boehmite consists of aluminum oxide-hydroxide with different amounts of H_2O molecules and various crystal sizes. In many cases, boehmite is the primary precursor for the synthesis of alumina phases. The physical and chemical characteristics of boehmite depend on the synthesis method. The crystal structure of boehmite is defined as the double chain of the AlO_6 octahedron. Pseudo-boehmite also consists of smaller crystals of boehmite that contain the same or similar octahedral layers. Carboxylate-alumoxane nanoparticles are characterized as the functionalized alumina nanostructure and are considered in the group of inorganic−organic hybrid materials.[36] Carboxylate-alumoxane nanoparticles can be applied for the synthesis of metal oxides,[37] catalytic materials,[38] preparation of ceramic membranes,[36] biocompatible nanocomposites,[39] and improvement

https://dx.doi.org/10.1021/acsomega.0c01732
ACS Omega 2020, 5, 16149−16164

of the performance of lithium-ion batteries.[40] The general chemical formula of carboxylate-alumoxane is $[Al(O)_x(OH)_y(O_2CR)_z]_n$, which shows that there are hydrophilic and hydrophobic parts in this nanostructure.[36,41,42] Al and O atoms induce the hydrophilicity behavior, and they can have interactions with heteroatoms of asphaltene molecules and provide hydrogen bondings with H−O, H−N, and H−S functional groups of asphaltene, respectively.[32] On the other hand, the alkyl chain (CR) part of this nanostructure, which contains the alkyl and resonance structures, provides the hydrophobicity behavior of carboxylate-alumoxane nanoparticles.[43] Regarding these chemical characteristics, carboxylate-alumoxane nanoparticles have been selected as a promising nanomaterial for the asphaltene adsorption and the postponement of asphaltene precipitation in this study.

To evaluate the asphaltene adsorption of carboxylate-alumoxane nanoparticles, adsorption experiments were performed with the spectroscopy technique. For detecting the onset of asphaltene precipitation and simultaneously measuring the amount of precipitated asphaltene, the indirect method,[44] which is a combination of spectroscopy and gravimetric techniques, was utilized. In comparison with other methods applied for determining the onset of asphaltene precipitation, this technique is sensitive, and it can be used for the experiments utilizing various ranges of asphaltene concentration. According to the indirect method, the onset point of asphaltene precipitation was determined by the difference in the optical properties of various samples with and without applying carboxylate-alumoxane nanoparticles.[44−46]

2. RESULT AND DISCUSSION

2.1. Characterization of Functionalized Nanoparticles. The sol−gel method was employed for the synthesis of carboxylate-alumoxane nanoparticles. The pH is considered as the most crucial factor affecting the size of functionalized nanoparticles in this technique. To produce PBMA and BMA nanoparticles, the pH was set at 3. Due to the fact that the pH augmentation results in the attachment of fewer carboxylate groups on the surface of nanoparticles, carboxylate-alumoxane nanoparticles will be agglomerated by increasing the pH value, causing a growth in the nanoparticle size.[47] For specifying the morphology of functionalized nanoparticles, FE-SEM images were prepared. Figure 2a shows the FE-SEM image of boehmite. The BMA morphology, which is attached nanosheets, is shown in Figure 2b. Figure 2c also shows the FE-SEM of pseudo-boehmite. In addition, the agglomerated nanoparticles are ascribed to the PBMA nanoparticles (Figure 2d). The difference between the two morphologies can be relevant to various structural characteristics associated with the raw precursors of two functionalized nanoparticles.

DLS analysis was carried out by the Malvern ZS Nano analyzer (Malvern Instrument Inc., London, U.K.) to identify the size distribution of functionalized nanoparticles. Figure 3 shows that the size distributions for PBMA and BMA are 12−35 and 32−155 nm, respectively. Additionally, as can be seen, the size distribution peaks for PBMA and BMA are around 21 and 74 nm, respectively.

For confirming the existence of functional groups on the surface of carboxylate-alumoxane nanoparticles, the FT-IR test was carried out. Figure 4a exhibits the FT-IR curves of boehmite and pseudo-boehmite. Figure 4b also shows the FT-IR curves of synthesized carboxylate-alumoxane nanoparticles. After evaluating the FT-IR analysis of PBMA, it is concluded

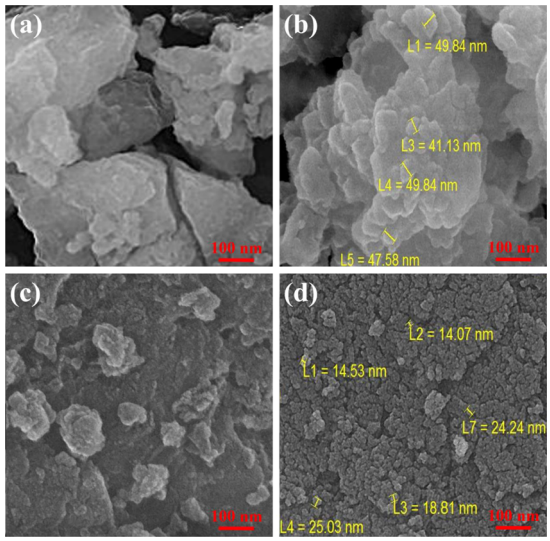

Figure 2. FE-SEM images of (a) boehmite, (b) BMA, (c) pseudo-boehmite, and (d) PBMA.

that at wavenumbers of 1473 and 1593 cm^{-1}, there are stretching vibrations that correspond to the C−O and C═O bonds. Moreover, the C−O−C (1260 and 1150 cm^{-1}), Al−OH (1071 and 989 cm^{-1}), and Al−O (430−740 cm^{-1}) bonds, which exist in the carboxylate functional groups and the carboxylate-alumoxane core, respectively, are observed in the FT-IR diagram. The C−H bonding is also confirmed in the wavenumber of 3090 cm^{-1}. The O−H peak is also exhibited in the range of 3310−3720. In Figure 4b, similar results related to C−O (1470 cm^{-1}), C═O (1590 cm^{-1}), C−O−C (1262 cm^{-1}), Al−OH (1060−970 cm^{-1}), Al−O (430−690 cm^{-1}), C−H (2932 cm^{-1}), and O−H (3453−3697 cm^{-1}) bonds can be seen in the FT-IR diagram of BMA nanoparticles. These results are consistent with the literature.[48]

Figure 5a exhibits the XRD patterns of boehmite and pseudo-boehmite. Figure 5b also manifests the XRD patterns of BMA and PBMA. By comparing the patterns of PBMA and BMA, it can be seen that these patterns are similar in respect to their peaks. Due to the fact that the compositions of boehmite and pseudo-boehmite are comparable, it is expected that the formed phases of these two functionalized nanoparticles will be the same. By comparing the XRD patterns of PBMA and BMA with the patterns obtained from different phases of alumina,[49] it is observed that the α-Al_2O_3, β-Al_2O_3, and γ-Al_2O_3 phases are formed. The peaks related to γ-AlOOH, α-$Al(OH)_3$, and elemental Al are also observed.

The surface areas resulting from BET analysis are 127 and 240 m^2/g for BMA and PBMA, respectively.[50] The total pore volumes are also 0.15 and 0.25 cm^3/g for BMA and PBMA, respectively. For these nanoparticles, the nitrogen adsorption−desorption isotherms were also prepared. Figure 6a shows the nitrogen adsorption−desorption isotherm of BMA. The hysteresis ring illustrates the type four isotherm in the curve. This type of isotherm indicates that BMA contains mesopores.[51] Moreover, Figure 6b shows the pore size distribution for BMA and reveals that the most commonly observed size of the pores is 1.64 nm.

Figure 7a also shows the nitrogen adsorption−desorption isotherm of PBMA. This isotherm is a mixture of type one and type four isotherms. The hysteresis ring shows the type four isotherm in the curve. This type of isotherm presents that

https://dx.doi.org/10.1021/acsomega.0c01732
ACS Omega 2020, 5, 16149−16164

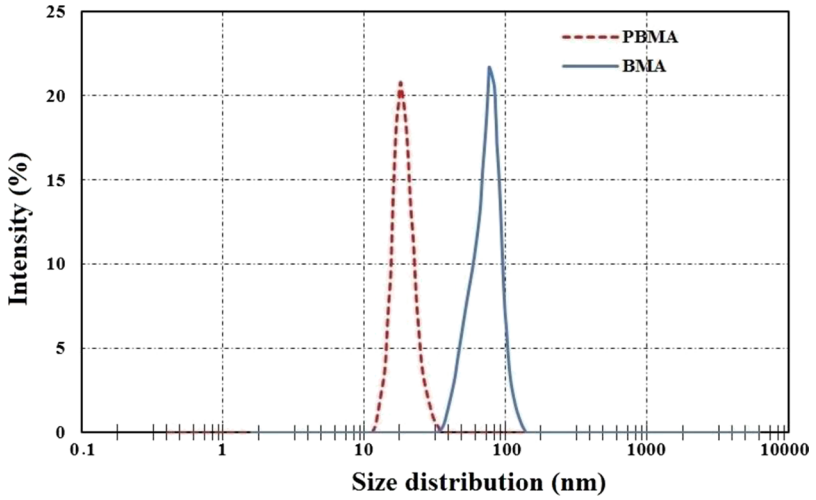

Figure 3. DLS analysis of BMA and PBMA nanoparticles.

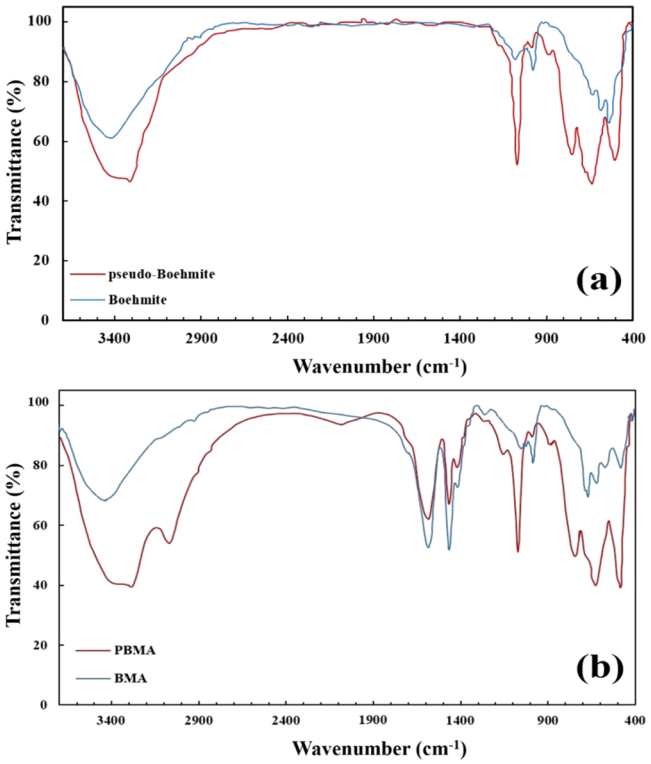

Figure 4. FT-IR analyses for (a) boehmite and pseudo-boehmite and (b) BMA and PBMA.

PBMA has both micropores and mesopores.[52] Figure 7b shows the pore size distribution for PBMA and reveals that the most occurring size of the pores is 2.41 nm. As can be seen, the surface area of PBMA nanoparticles is higher than this characteristic for BMA, which may be contributed to the existence of more functional groups on the surface of PBMA nanoparticles. Thus, the interactions between PBMA and asphaltene molecules may be higher than BMA nanoparticles in the same conditions.

2.2. Adsorption Capacity Experiments Results. To perform the adsorption capacity experiments, 500 ppm synthetic oil samples were prepared, one of which was the reference (without nanoparticles) and the remaining samples were the synthetic oils that consist of specific amounts of PBMA and BMA. Figure 8 shows the relationship between the carboxylate-alumoxane nanoparticle amount and adsorption capacity as well as adsorption efficiency. The results illustrate that with respect to the increment in nanoparticle concentration, asphaltene adsorption efficiency is increasing. However, as can be seen in Figure 8, the adsorption capacity of these nanoparticles is reduced when the amount of nanoparticles increases. Based on Figure 8, for 0.1 wt % PBMA nanoparticles, the adsorption capacity is 78.4 mg/g. By increasing the amount of PBMA nanoparticles to 0.4 wt %, the adsorption capacity amount reaches 31.4 mg/g, indicating adsorption capacity reduction of about 60%. However, by studying the asphaltene adsorption efficiency related to PBMA nanoparticles, the adsorption efficiency augments from 15.6 to 25.2% with the increment of PBMA nanoparticles from 0.1 to 0.4 wt %, respectively. In addition, the adsorption capacity behavior of BMA nanoparticles is displayed in Figure 8. For this functionalized nanoparticle, with increasing nanoparticle concentration, the adsorption capacity also decreases along with the increment in asphaltene adsorption efficiency. From 0.1 to 0.4 wt % concentration of BMA nanoparticles existing in synthetic oil, the adsorption capacity is measured to be 64.2 to 22.4 mg/g, respectively, which manifests a reduction around 40 to 65% with increasing concentration of the BMA nanoparticles.

According to the evidence mentioned in the paragraph above, it is concluded that with the increment in carboxylate-alumoxane nanoparticle concentration, the adsorption sites for the interaction of asphaltenes and nanoparticles are augmented, resulting in the enhancement of asphaltene adsorption efficiency. These results are consistent with the literature.[53−56] The reason for the reduction in adsorption capacity of two nanoparticles in terms of the nanoparticle dosage is that at 0.1 wt % of nanoparticles, asphaltene molecules have a tendency to distribute over the whole surface of the nanoparticles, and consequently, they attempt to occupy more sites of the adsorbent surface. By increasing the mass of nanoparticles, asphaltene is attracted to a higher surface amount of adsorbent, which results in the less asphaltene adsorption on the unit mass of nanoparticles.[57] Furthermore, particulate interactions can be assumed as another reason for this phenomenon. In other words, the higher concentration of nanoparticles will intensify their aggregation potentiality, which not only causes a

https://dx.doi.org/10.1021/acsomega.0c01732
ACS Omega 2020, 5, 16149−16164

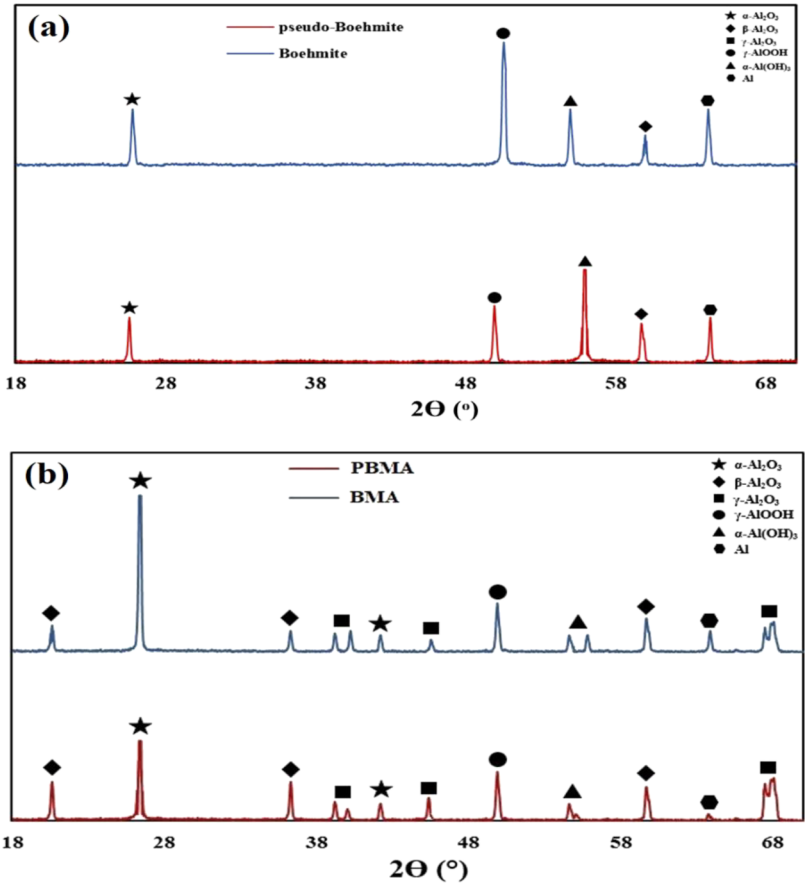

Figure 5. XRD analyses for (a) boehmite and pseudo-boehmite and (b) BMA and PBMA.

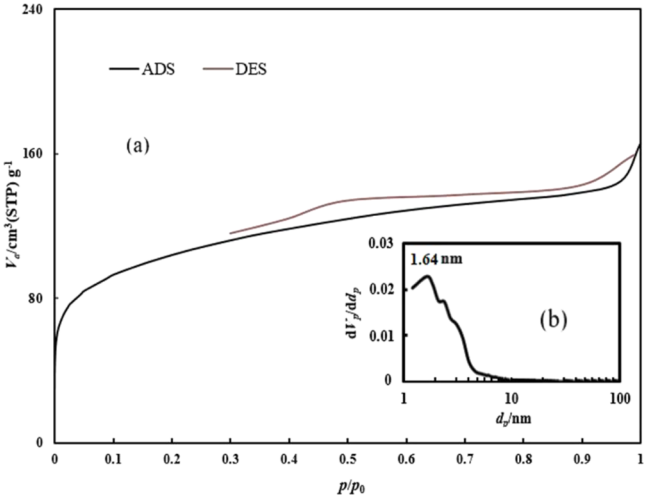

Figure 6. (a) Nitrogen adsorption−desorption isotherm and (b) pore size distribution for BMA.

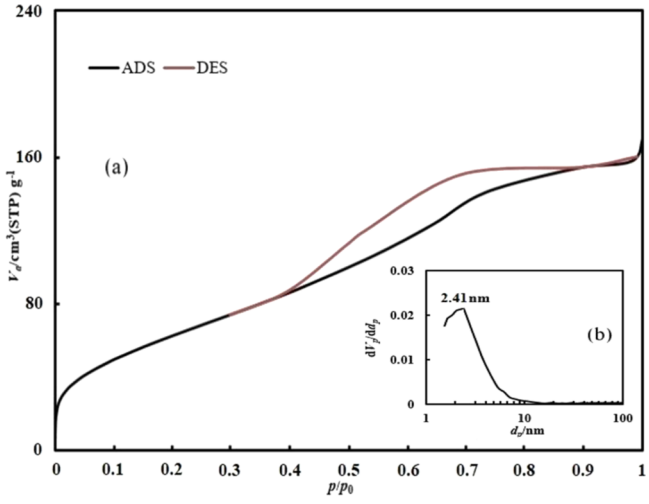

Figure 7. (a) Nitrogen adsorption−desorption isotherm and (b) pore size distribution for PBMA.

reduction in the overall adsorbent surface area but also increases the diffusional path length. Consequently, most of the adsorption sites associated with functionalized nanoparticles overlap, and this factor results in the mass transfer diminution due to the interfacial tension augmentation between adsorbent and liquid phases.[58] Therefore, due to the high concentration of nanoparticles, the weak interactions between nanoparticles and asphaltene molecules may be removed, assisting the desorption of asphaltene molecules from the surface of carboxylate-alumoxane nanoparticles.

By investigation of the results from Figure 8, it is established that the adsorption capacity, as well as the adsorption efficiency, is higher for PBMA compared with BMA nanoparticles in the same concentrations. These results can be attributed to two important reasons. The first reason is related to the difference ascribed to the size of two nanoparticles. As mentioned in Sections 2.1 and 2.2, PBMA nanoparticles possess a smaller size in comparison with BMA nanoparticles. This vital characteristic assists them in having better dispersion in liquid phases, inducing more interactions with asphaltenes in

https://dx.doi.org/10.1021/acsomega.0c01732
ACS Omega 2020, 5, 16149−16164

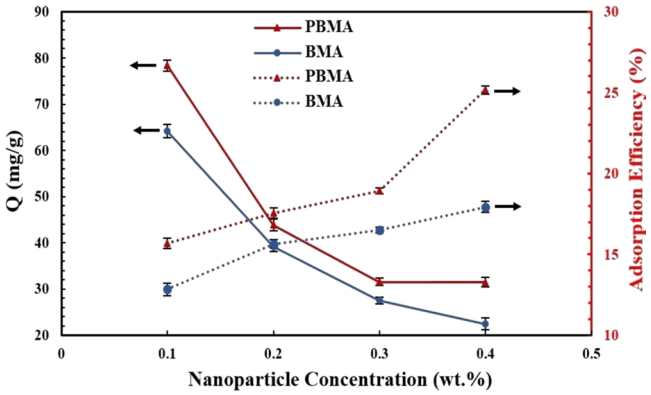

Figure 8. Adsorption capacity and adsorption efficiency of two nanoparticles toward asphaltene adsorption (500 ppm synthetic oil) in various concentrations of nanoparticles.

synthetic oil.[59−63] Another reason for this phenomenon can be ascribed to the surface area of nanoparticles. Due to the fact that the surface area of PBMA is higher than BMA, it can provide an opportunity for PBMA to expose more of their body surface to asphaltene molecules, causing greater adsorption capacity.[64]

Based on this investigation, the concentration of 0.1 wt % was selected for performing the asphaltene precipitation experiments. That is because the overall cost related to the adsorbent preparation compared with the adsorption capacity can be diminished. Additionally, by employing this concentration, the risk of nanoparticle aggregation, which contributes to the obstruction of the reservoir pore space and oil production prevention, can be reduced.[65]

Moreover, Figure 9 exhibits the adsorption capacity of two carboxylate-alumoxane nanoparticles for various synthetic oils

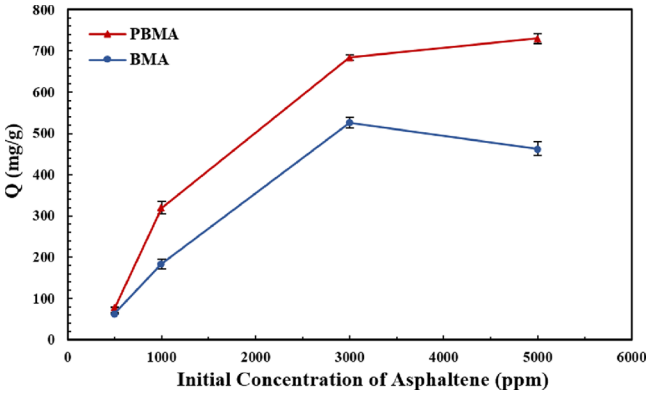

Figure 9. Adsorption capacity of two nanoparticles (0.1 wt %) toward asphaltene adsorption in various initial concentrations of asphaltenes (500, 1000, 3000, and 5000 ppm).

with asphaltene concentrations of 500, 1000, 3000, and 5000 ppm. Figure 9 clarifies that for a specific mass of PBMA nanoparticles (0.1 wt %), the asphaltene adsorption capacity is intensified by the asphaltene concentration augmentation. However, by increasing the asphaltene concentration, the slope of curve related to the adsorption capacity value in different initial concentrations of asphaltene declines. Additionally, BMA nanoparticles have a behavior similar to PBMA nanoparticles in 500 to 3000 ppm asphaltene concentrations. Conversely, the adsorption capacity of BMA decreases in 3000 to 5000 ppm asphaltene concentrations.

By evaluating the results mentioned in the paragraph above, it is concluded that by increasing the asphaltene concentration in synthetic oils with a constant concentration of carboxylate-alumoxane nanoparticles, the adsorption sites of nanoparticles exposed to asphaltene molecules are reduced, resulting in the reduction of adsorption capacity slope. Furthermore, with the increment in asphaltene concentrations in various samples, the size of aggregated asphaltenes is augmented due to a more promising asphaltene self-association, which contributes to the diffusion restriction for asphaltene molecules that tend to be adsorbed on the surface of carboxylate-alumoxane nanoparticles.[34,64,66]

2.3. Adsorption Isotherm Models. The investigation of adsorption isotherms is useful for describing the interaction between asphaltene molecules and carboxylate-alumoxane nanoparticles. Choosing appropriate isotherm equations can assist the system in being optimized while designing the adsorption process. In this study, among several isotherm models, two well-known isotherm equations, including Langmuir and Freundlich isotherm models, were selected. The linear form of the Langmuir isotherm equation is exhibited in eq 1.[67]

$$\frac{C_e}{Q_e} = \frac{C_e}{Q_m} + \frac{1}{Q_m K_L} \quad (1)$$

where Q_e is the equilibrium adsorption capacity of nanoparticles (mg/m^2), Q_m is the maximum adsorption capacity (mg/m^2) related to the maximum monolayer capacity, C_e is the equilibrium concentration of asphaltene (mg/L), and K_L is the Langmuir constant parameter associated with the affinity of binding sites.

The linear form of the Freundlich isotherm equation is also shown in eq 2.[68] In this equation, K_f is the Freundlich constant parameter, and $\frac{1}{n_f}$ is the slope of the curve resulting from plotting LogQ_e versus LogC_e.

$$\text{Log } Q_e = \text{Log } K_f + \frac{1}{n_f}\text{Log } C_e \quad (2)$$

Figure 10a,b shows the Langmuir and Freundlich isotherm plots, respectively, for adsorption of asphaltene onto the BMA and PBAM nanoparticles. The Langmuir and Freundlich parameters can be seen in Table 1. The Langmuir model suggests that adsorption phenomena occur with a monolayer arrangement on the surface of nanoparticles, and thus, the adsorbed molecules do not interact with each other. On the other hand, the Freundlich isotherm model assumes that molecules are adsorbed as a monolayer or multilayer on the heterogeneous surface of nanoparticles, the adsorbed molecules interact with each other, and the adsorption sites have various adsorption energies.[69,70] Based on the results of Figure 10a,b and Table 1, it is concluded that the data, which results from the adsorption of asphaltene on the surface of nanoparticles, is better fitted to the Freundlich isotherm model than the Langmuir model. As can be seen, the coefficients of determination (R^2) resulting from the Freundlich isotherm plots are 0.936 and 0.865 for PBAM and BMA, respectively. However, these values, which result from the Langmuir model, are 0.817 and 0.714 for PBAM and BMA, respectively. Based on the Langmuir model, the Q_m

https://dx.doi.org/10.1021/acsomega.0c01732
ACS Omega 2020, 5, 16149−16164

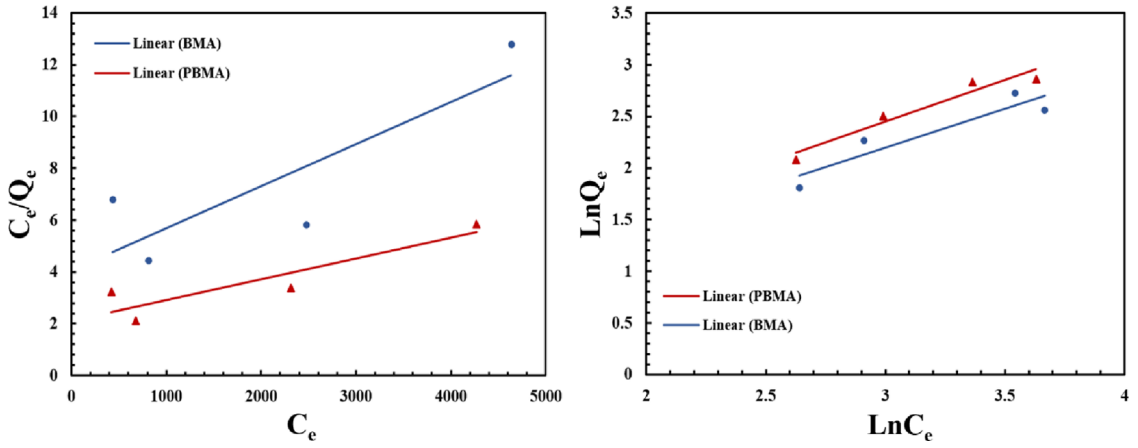

Figure 10. Linear isotherm plots for (a) Langmuir adsorption isotherm and (b) Freundlich adsorption isotherm of asphaltenes onto two different carboxylate-alumoxane nanoparticles.

Table 1. Langmuir and Freundlich Isotherm Constant for Asphaltene Adsorption on the Surface of Nanoparticles

	Langmuir isotherm			Freundlich isotherm		
nanoparticle	Q_m (mg/m^2)	K_L	R^2	K_f	$1/n_f$	R^2
PBMA	5.21	0.091	0.817	1.07	0.806	0.936
BMA	4.92	0.050	0.714	0.67	0.756	0.865

values are 5.21 and 4.92 mg/m^2 for PBAM and BMA, respectively, and these values indicate that the maximum adsorption capacity (mg/m^2) related to the maximum monolayer capacity for PBAM is higher than this value for BMA. Moreover, according to the Freundlich isotherm model, the adsorption of asphaltene on BMA and PBAM is favorable because of $\frac{1}{n_f} < 1$.[71]

2.4. Impact of Functionalized Nanoparticles on the Onset of Asphaltene Precipitation. For investigating the inhibitory performance of two types of carboxylate-alumoxane nanoparticles, first, determining the onset point of asphaltene precipitation for a synthetic oil with 1000 ppm asphaltene was performed without the existence of carboxylate-alumoxane nanoparticles via the indirect technique. According to Figure 11a, there is a linear trend for the absorbance values measured for supernatants in terms of *n*-heptane vol % from 0 to 50%. At the point of 60 vol % *n*-heptane, the curve deviates from the linear trend, indicating that the Beer−Lambert law is not valid anymore. These results imply that the onset point of asphaltene precipitation for the reference synthetic oil including 1000 ppm asphaltene occurs in 50 vol % *n*-heptane. Figure 11b shows the data resulting from measured absorbance after correcting the dilution impact. In the rest of this paper, all of the results are presented by considering the measured absorbance modification. Considering Figure 11b, the changes in absorbance value from 1.53 to 1.42 for 0 to 50 vol % *n*-heptane, respectively, can be justified. Based on these results, there is no considerable absorbance reduction in this range. From 50 to 60 vol % *n*-heptane, the absorbance value decreases to 1.14, which confirms the abrupt deviation. To confirm 50 vol % *n*-heptane as the onset point of asphaltene precipitation and continuous deviation after the onset point, four midpoints between 50−60 and 60−70 vol % were selected. By evaluating these midpoints exhibited in Figure 12, 50 vol % *n*-heptane is validated for the onset point of precipitation for synthetic oil with 1000 ppm asphaltene. Figure 12 manifests the onset point of asphaltene precipitation in the presence of PBMA and BMA nanoparticles compared with the reference synthetic oil. By considering this figure, it can be confirmed that the onset of

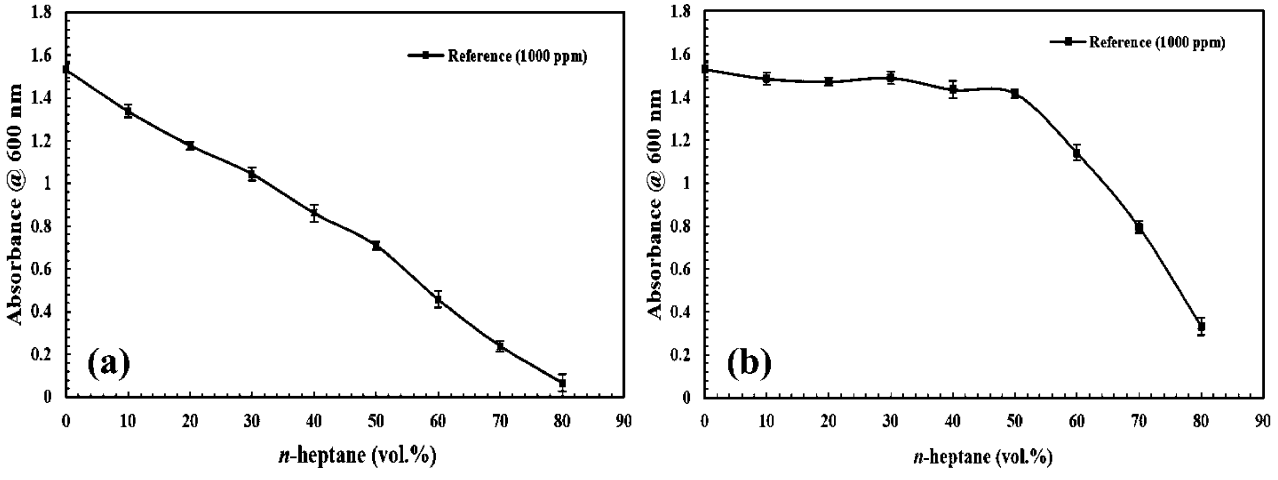

Figure 11. Onset point determination for the reference synthetic oil (1000 ppm asphaltene) (a) before dilution impact correction and (b) after dilution impact correction.

https://dx.doi.org/10.1021/acsomega.0c01732
ACS Omega 2020, 5, 16149−16164

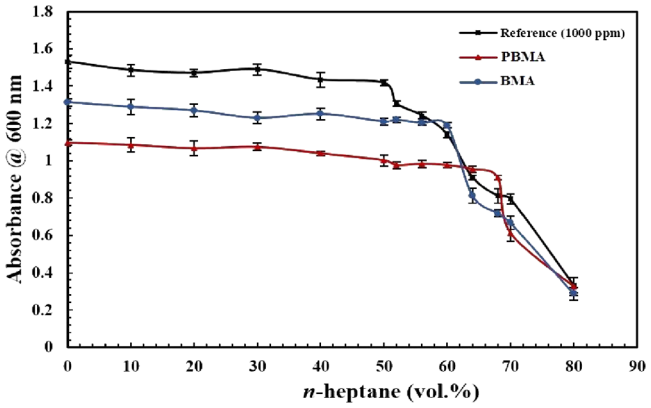

Figure 12. Onset point determination for the synthetic oil (1000 ppm asphaltene) in the absence and presence of carboxylate-alumoxane nanoparticles (0.1 wt %) after dilution impact correction.

asphaltene precipitation occurs in 60 vol % *n*-heptane in the presence of BMA nanoparticles. On the other hand, the performance of PBMA is different from the BMA impact. By investigating the outcomes indicated by Figure 12, it is justified that the onset point of precipitation when PBMA is present in the synthetic oil should be considered in the 68 vol % precipitant. For clarification of the effects of the nanoparticles on asphaltene precipitation in comparison with the reference synthetic oil, the differences among their onset points were calculated. The postponements in the onset point of precipitation by the utilization of BMA and PBMA are 17 and 26%, respectively, compared with the onset point of the reference synthetic oil. As can be seen, the existence of PBMA and BMA plays a positive role in postponing the precipitation of asphaltene in synthetic oil. Additionally, Figure 12 also manifests a reduction in the absorbance value in the presence of nanoparticles. Not only is this reduction viewed at before the instability point, but it is also revealed after the onset point of precipitation. The absorbance values in the onset point for BMA and PBMA are 1.2 and 0.91, respectively.

The reduction in the absorbance value corresponds to the elimination of asphaltene from synthetic oil. The most crucial factor for asphaltene removal in the presence of carboxylate-alumoxane nanoparticles is the adsorption of asphaltene on the surface of these functionalized nanoparticles.[33,72] After the centrifugation process, the carboxylate-alumoxane nanoparticles containing asphaltene are removed from the system. Therefore, this asphaltene removal changes the optical properties of synthetic oils. This asphaltene elimination from synthetic oil contributes to the decrement in asphaltene concentration in various types of synthetic oils. Because of the higher concentration of asphaltene, asphaltene precipitation occurs sooner than in conditions in which the asphaltene amount is small. Thus, the delay in the onset point of asphaltene precipitation takes place, while lower asphaltene concentration exists in the synthetic oil. On account of the fact that the adsorption of asphaltene on the surface of nanoparticles assists in the stability of asphaltene in the oil reservoirs,[10,73] the indirect method exhibits the potentiality of nanoparticles in the postponement of asphaltene precipitation indirectly by indicating the changes in the optical properties of various synthetic oils.[44−46]

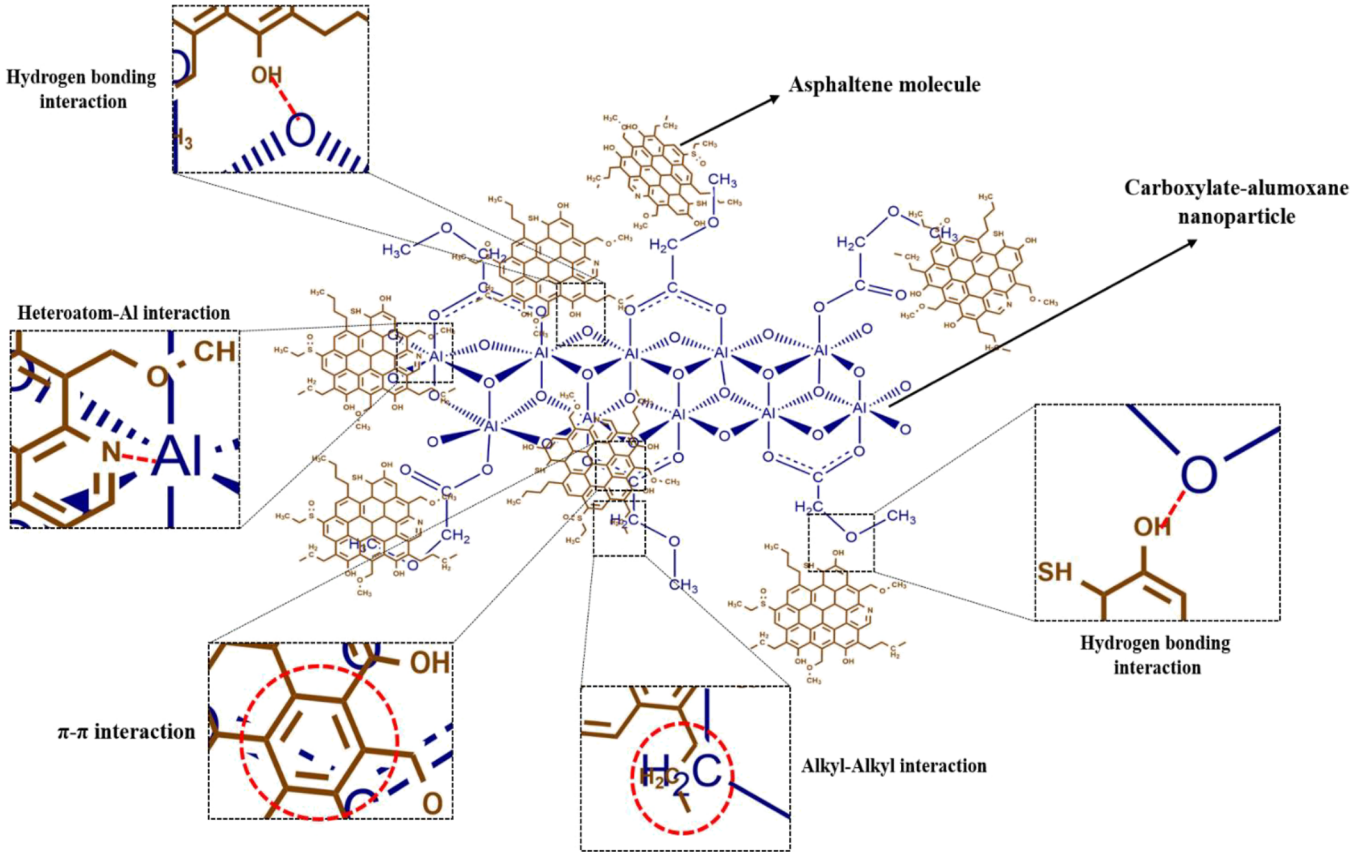

Figure 13. Schematic of the proposed mechanisms for asphaltene molecules adsorption on the surface of carboxylate-alumoxane nanoparticles.

https://dx.doi.org/10.1021/acsomega.0c01732
ACS Omega 2020, 5, 16149−16164

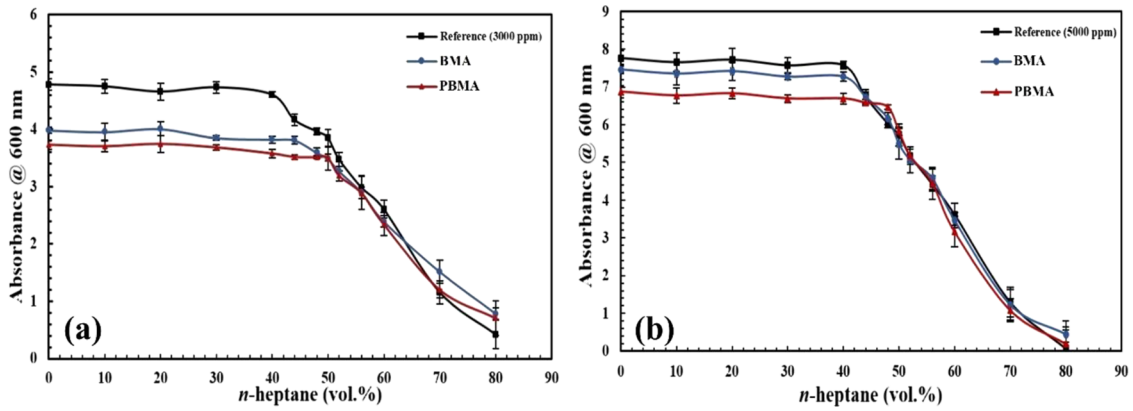

Figure 14. Onset point determination for two synthetic oils with (a) 3000 ppm asphaltene and (b) 5000 ppm asphaltene in the absence and presence of carboxylate-alumoxane nanoparticles (0.1 wt %) after dilution impact correction.

There are some mechanisms related to the structure of carboxylate-alumoxane nanoparticles for the asphaltene adsorption. Figure 13 exhibits the proposed mechanisms for the asphaltene molecule adsorption. The first mechanism corresponds to hydrogen bonding created between carboxylate-alumoxane nanoparticles and asphaltene molecules. Since there are H−O, H−N, and H−S functional groups in the structure of asphaltene molecules, hydrogen atoms existing in these functional groups have a high tendency to generate interactions with the oxygen atoms in the carboxylate-alumoxane core.[32,72,74] As can be seen in Figure 1, there are a large number of oxygen atoms in the carboxylate-alumoxane network. Thus, this factor should open up an exceptional opportunity for asphaltene molecules to be adsorbed on the surface of carboxylate-alumoxane nanoparticles. Additionally, with respect to having oxygen atoms in their molecular structure, carboxylate functional groups attached on the surface of carboxylate-alumoxane nanoparticles provide a vital chance for asphaltene molecules to generate other hydrogen bonding interactions. According to these functional groups, the hydrogen atoms of H−O, H−N, and H−S functional groups related to the asphaltene structure can construct the hydrogen bonds with oxygens existing in ether and carbonyl functional groups attributed to carboxylate functional groups. Consequently, the adsorption of asphaltenes on the surface of nanoparticles will be intensified. The second mechanism can be ascribed to the interactions between heteroatoms, including N, O, and S atoms in the structure of asphaltenes, and Al atoms, which locate in the carboxylate-alumoxane core. These Al atoms can act as Lewis acids, and the heteroatoms existing in the asphaltene structure play a Lewis base role.[32,72,75,76] This phenomenon can cause the interactions between numerous Al atoms and the heteroatoms of asphaltene molecules, facilitating the adsorption process. Moreover, the resonance structures associated with the attachment points of carboxylate functional groups and the carboxylate-alumoxane core can also facilitate the adsorption process. Regarding the generation of $\pi-\pi$ interactions, these resonance structures can create strong interactions with the aromatic rings belonging to asphaltene structures.[43,77] The $\pi-\pi$ interactions can sometimes provide potent interactions between adsorbents and adsorbates, causing the increased adsorption phenomenon. Finally, the presence of CH_3- and $-CH_2-$ in the functional groups of carboxylate-alumoxane nanoparticles may cause hydrophobic interactions (alkyl−alkyl and alkyl−π) with the alkyl chains and aromatic rings of asphaltene, which may result in dispersion forces.[78]

According to the results from the experiments of determining the onset point of asphaltene precipitation, PBMA nanoparticles exhibit more effective performance in comparison with BMA nanoparticles. As mentioned in Sections 2.1 and 2.2, PBMA nanoparticles possess a higher surface area compared with BMA nanoparticles. This vital characteristic will contribute more adsorption sites for PBMA nanoparticles to adsorb more asphaltene molecules. In addition, with respect to this higher surface area, PBMA nanoparticles possess more attached functional groups in comparison with BMA nanoparticles. Consequently, the more functional groups existed on the surface of nanoparticles, the more the interactions that occur between PBMA and asphaltene molecules, leading to higher adsorption capacity for PBMA nanoparticles. On the other hand, the size of the PBMA nanoparticles is smaller than BMA nanoparticles. Due to this property, PBMA can be further dispersed in synthetic oil, and these nanoparticles can have more diffusion among asphaltene molecules, which contributes to better interactions with asphaltenes in comparison with BMA. Thus, PBMA provides better performance in postponing the asphaltene precipitation.

2.5. The Effect of Carboxylate-Alumoxane Nanoparticles on a Higher Asphaltene Concentration. For the assessment of the effect of BMA and PBMA nanoparticles on higher concentrations of asphaltenes, the previous experiments were carried out for two synthetic oils containing 3000 and 5000 ppm asphaltene. Figure 14a discloses the results obtained from determining the onset point of asphaltene precipitation for 3000 ppm synthetic oil by using the indirect technique. Based on this figure, the deviation from the linear trend attributed to the asphaltene precipitation onset point occurs in the 40 vol % precipitant for the reference synthetic oil. As can be seen, the onset point occurs in lower *n*-heptane vol % in comparison with Figure 12 related to the 1000 ppm synthetic oil. The absorbance values for the reference synthetic oil (3000 ppm) in 0 and 40 vol % precipitants are 4.7 and 4.6, respectively, which demonstrates that with increasing asphaltene concentration, the absorbance values are also increased based on linear dependency. The curves related to the presence of two different carboxylate-alumoxane nanoparticles are plotted in Figure 14a. These curves also demonstrate that the onset points for the samples consisting of PBMA and BMA

https://dx.doi.org/10.1021/acsomega.0c01732
ACS Omega 2020, 5, 16149−16164

are 50 and 44 vol % *n*-heptane with the absorbance values of 3.5 and 3.8, respectively. By assessing the difference in the absorbance values between the reference and nanoparticles for 1000 and 3000 ppm synthetic oil, it is observed that the gaps existing in synthetic oil with 3000 ppm asphaltene are lower than this variation in the synthetic oil, which includes 1000 ppm asphaltene. The differences in the presence and absence of nanoparticles are about 20 and 9% for PBMA and BMA, respectively, in comparison with the reference synthetic oil with 3000 ppm asphaltene. Thus, it is concluded that in a higher concentration of asphaltenes, the performance of PBMA and BMA decreases when their concentration is identical for the amounts of nanoparticles applied in the lower concentration of asphaltene. For the synthetic oil with 5000 ppm asphaltene, the onset points exhibited in Figure 14b are 40, 40, and 48 vol % of precipitants with the absorbance values of 7.5, 7.3, and 6.4 in the absence of carboxylate-alumoxane nanoparticles, in the presence of BMA and PBMA, respectively. By considering the data resulting from this experiment, it is approved that with the increment in asphaltene concentration, the impact of BMA nanoparticles in postponing the onset point of asphaltene precipitation can be neglected for 5000 ppm asphaltene concentration. On the other hand, the PBMA nanoparticles also modify the onset point to about 17% compared with the onset point achieved from the reference synthetic oil. With the investigation of absorbance value, it is perceived that the difference between the absorbance values of the reference and synthetic oil with BMA nanoparticles is small, and thus, it does not provide the opportunity to postpone the onset point of asphaltene precipitation. However, the absorbance value of the sample with PBMA demonstrates that its difference from the absorbance value of the reference is significant for the asphaltene precipitation postponement. The most important reason for this phenomenon is that by increasing the asphaltene concentration, the self-association of asphaltene molecules is augmented, resulting in the reduction of carboxylate-alumoxane nanoparticle effect on the asphaltene adsorption.

2.6. Precipitated Asphaltene Amount. Figure 15 illustrates the precipitated asphaltene percentage of the synthetic oil containing 1000 ppm asphaltene in various vol % of *n*-heptane for the reference synthetic oil in the presence of PBMA and BMA nanoparticles. As observed, before the 50 vol % precipitant (the onset point for the reference synthetic oil), the precipitated asphaltene percentage is almost equal for the three samples. By considering Figure 15, it is also observed that the difference in the asphaltene precipitated amount in the presence of BMA and without this functionalized nanoparticle is 17% in the 60 vol % precipitant, which is the onset point of the synthetic oil with BMA. On the other hand, in the presence of PBMA, this difference is calculated to be 36% in the 68 vol % precipitant, indicating that PBMA has better performance in the inhibition of asphaltene precipitation in comparison with BMA nanoparticles. Figure 16a,b also demonstrates the aggregated asphaltene amount for the synthetic oils with 3000 and 5000 ppm asphaltene, respectively. Figure 16a indicates that the differences in precipitated amount for BMA and PBMA in comparison with the reference synthetic oil were measured to be 8 and 13% in 44 and 50 vol % precipitants, respectively. The data observed from Figure 16b also established the fact that the difference in the precipitated asphaltene amount for the sample containing BMA is insignificant compared with the 5000 ppm reference synthetic oil in 40 vol % *n*-heptane. Nonetheless, this value for the synthetic oil, which consists of PBMA, is 11% in the 48 vol % precipitant.

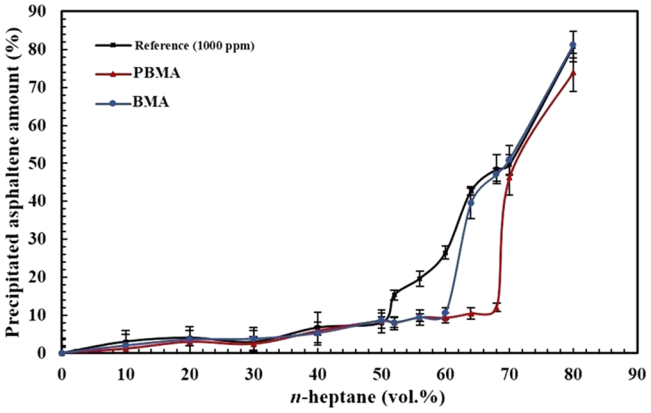

Figure 15. Precipitated asphaltene amount for the synthetic oil (1000 ppm asphaltene) in the absence and presence of carboxylate-alumoxane nanoparticles (0.1 wt %) after dilution impact correction.

As a consequence, the results obtained from the amount of precipitated asphaltene confirm the data resulting from the onset point of asphaltene precipitation. By comparing Figures 15 and 16, it is evident that by the increment in asphaltene concentrations, sudden precipitation happens in a lower volume percentage of precipitant. Additionally, the differences between precipitated asphaltene amounts in the presence of nanoparticles and in the absence of nanoparticles diminish while the asphaltene concentration increases. As a result, the inhibitory performance of carboxylate-alumoxane nanoparticles decreases when the asphaltene concentration is augmented. The varieties related to the precipitated amount of asphaltene in the same vol % of *n*-heptane obviously reveal the better application of PBMA nanoparticles in the inhibitory performance. These results are attributed to the various adsorption capacities of these nanoparticles, which are consistent with their size distribution as well as their specific surface area. As stated in previous sections, regarding smaller size, as well as higher surface area, PBMA can provide more resistance against abrupt precipitation of asphaltene compared with BMA nanoparticles due to creation of more interactions with asphaltene molecules, which contributed to more asphaltene adsorption in the synthetic oil having the same concentrations. This adsorption ability results in more asphaltene stability in synthetic oil, which is exhibited by an indirect technique via the optical property variations of different samples.

3. CONCLUSIONS

In this research, the effect of carboxylate-alumoxane nanoparticles (PBMA and BMA), which were considered as functionalized nanoparticles, was studied on the inhibition of asphaltene precipitation. The adsorption capacity experiments of these nanoparticles clarified that with increasing concentration of PBMA and BMA, their asphaltene adsorption efficiency increases because of the existence of more adsorption sites by the increment in nanoparticles dosage. However, the adsorption capacity of two nanoparticles decreases due to the augmentation of the particulate interactions among nanoparticles as well as mass transfer reduction. Adsorption capacity experiments reveal that PBMA

https://dx.doi.org/10.1021/acsomega.0c01732
ACS Omega 2020, 5, 16149−16164

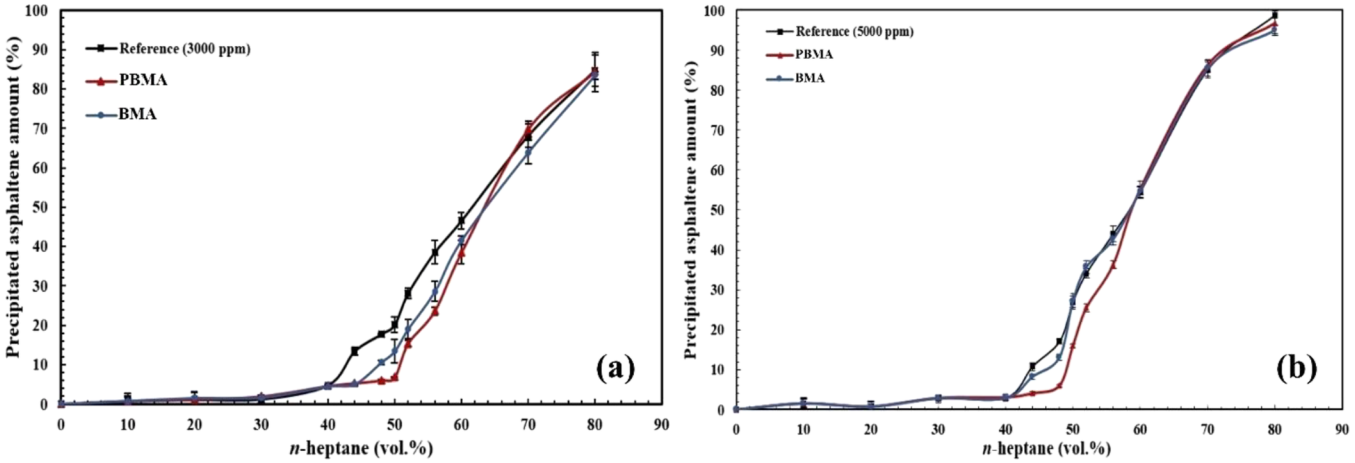

Figure 16. Precipitated asphaltene amount for two synthetic oils with (a) 3000 ppm asphaltene and (b) 5000 ppm asphaltene in the absence and presence of carboxylate-alumoxane nanoparticles (0.1 wt %) after dilution impact correction.

exhibits higher adsorption capacity, as well as higher adsorption efficiency, compared with BMA because of having a smaller size and higher surface area. Furthermore, the adsorption experiments illustrated that with augmentation of the asphaltene initial concentration in various synthetic oils containing a constant mass of carboxylate-alumoxane nanoparticles, the adsorption capacity is intensified, although its slope has declined. Besides, carboxylate-alumoxane nanoparticles postpone the onset point of asphaltene precipitation via adsorption of asphaltene, which contributed to a lower precipitated asphaltene amount. In the presence of PBMA (0.1 wt %), the onset point was delayed around 26, 20, and 17% in the asphaltene concentrations of 1000, 3000, and 5000 ppm, respectively, in comparison with their reference synthetic oils. On the other hand, these postponements for BMA nanoparticles (0.1 wt %) were 17%, 9%, and insignificant for the asphaltene concentrations of 1000, 3000, and 5000 ppm, respectively. The mechanism of adsorption phenomenon can be attributed to molecular interactions, including hydrogen bonding, Lewis acid−base interactions, $\pi-\pi$ interactions, and hydrophobic interactions. Furthermore, PBMA manifested a better inhibitory performance, which can be ascribed to its smaller size along with higher surface area, resulting in more adsorption sites for asphaltene molecules.

4. EXPERIMENTAL PROCEDURE

4.1. Material. To prepare the carboxylate-alumoxane nanoparticles, boehmite and pseudo-boehmite (manufactured by Sasol Company) were used as precursors. For the functionalization process, methoxyacetic acid (98%, Sigma-Aldrich, Taufkirchen, Germany) was employed via the sol−gel method. The asphaltene used in this study was extracted from crude oil that originated from one of the Iranian south oil reservoirs. The characteristics of this crude oil are reported in Table 2. The *n*-heptane utilized for asphaltene precipitation and purification was of reagent grade and was purchased from Merck-Millipore (99%). For the purification of asphaltene, as well as preparation of the synthetic oil, toluene (Mojallali Company, 99%, Tehran, Iran) was used.

Table 2. Crude Oil Properties Used in the Asphaltene Extraction Process

°API	μ (cp) @ 24 °C, 15 psia	saturates	aromatics	resins	asphaltenes
20.47	66.8055	43.4%	35.6%	12.9%	8.1%

4.2. Preparing Functionalized Nanoparticles. Carboxylate-alumoxane nanoparticles were synthesized according to our previous study[50] and the procedure used by Callender et al.[79] For producing PBMA, 7.5 g of pseudo-boehmite was mixed with deionized water (112.5 mL) and methoxyacetic acid (20 mL). For fixing the functional groups on the surface of nanoparticles, the mixture was kept under reflux for 12 h. The slurry resulting from the reflux process was centrifuged for 15 min at 5000 rpm. A vacuum oven (0.01 Torr), which was fixed at 60 °C, was employed for eliminating the volatiles from the resulting solution. Some white powders were produced at the end of the drying process. After that, by applying diethyl ether, the resulting powders were washed, followed by dispersion in 75 mL of ethanol. To precipitate PBMA nanoparticles, 225 mL of diethyl ether was added to the mixture. Afterward, the powders were dispersed in deionized water to eliminate the residual acid in three stages under vacuum, and then the solvent was removed with the help of the evaporation process. The synthesis procedure employed for producing BMA was the same as the procedure used in the synthesis of PBMA, with the difference being that the precursor used for BMA synthesis was boehmite. For preparing BMA, 7.5 g of boehmite was slowly added to 112.5 mL of deionized water and 20 mL of methoxyacetic acid. Then, it was put under reflux for 12 h. After the reflux process, for the separation of unreacted boehmite, the resulting slurry was centrifuged for 15 h at 5000 rpm. A vacuum oven (0.01 Torr), which was fixed at 60 °C, was used for eliminating the volatiles from the resulting solution. Some white powders were produced at the end of the drying process. After that, by applying diethyl ether, resulting powders were washed, followed by dispersion in 75 mL of ethanol. To precipitate BMA nanoparticles, 225 mL of ether was added to the mixture. Afterward, the powders were dispersed in deionized water to eliminate the residual acid in three stages under vacuum, and then the solvent was removed with the evaporation process. For characterizing the synthesized functionalized nanoparticles, various properties of nanoparticles were evaluated. To confirm the presence of carboxylate functional groups on the surface of synthesized nanoparticles, Fourier-transform infrared spectroscopy (FT-IR) test was conducted. Additionally, for studying the

https://dx.doi.org/10.1021/acsomega.0c01732
ACS Omega 2020, 5, 16149−16164

functionalized nanoparticle morphology, field-emission scanning electron microscopy (FE-SEM) images were prepared. The specific surface area was recognized via Brunauer–Emmett–Teller (BET) test. For determining the nano-alumina phases, X-ray diffraction (XRD) analysis was done. In addition, dynamic light scattering (DLS) test revealed the size distribution of functionalized nanoparticles investigated in this study.

4.3. Synthetic Oil Preparation. In this research, to evaluate the effect of carboxylate-alumoxane nanoparticles on asphaltene precipitation, different synthetic oils possessing various asphaltene concentrations were prepared. For this reason, specific amounts of pure asphaltene obtained from the ASTM (D6560)–IP143 asphaltene extraction technique (Section S1 in Supporting Information) were added to specific volumes of toluene. After that, the mixture was agitated with a magnetic stirrer for 1 h in order for the asphaltene to be solved completely in the toluene. In this study, one synthetic oil containing 500 ppm asphaltene for adsorption capacity experiments and three synthetic oils with concentrations of 1000, 3000, and 5000 ppm for conducting the tests related to adsorption capacity and the onset point of asphaltene precipitation were prepared. For approving the complete dissolution of asphaltene in toluene, different synthetic oils were then observed via a Nikon SE 200 transmitted-light microscope after preparation.

4.4. Adsorption Capacity Experiments. To perform the adsorption efficiency and adsorption capacity experiments of two different functionalized nanoparticles toward asphaltene adsorption, batch adsorption tests were carried out. For this purpose, specific amounts of two nanoparticles were dispersed in 500 ppm synthetic oils. To compare the effect of different concentrations of nanoparticles on the adsorption of asphaltene, synthetic oils consisting of 0.1, 0.2, 0.3, and 0.4 wt % of both PBMA and BMA were prepared. Different concentrations of two nanoparticles were dispersed in the synthetic oil by employing an ultrasonic disruptor (UP-400 A) from Ultrasonic Technology Development Co. (UTDC), which was set at the power of 150 W. Afterward, the samples were transferred into sample tubes and then the tubes were sealed properly to avoid the loss of toluene by evaporation and left for 2 h at an ambient pressure and temperature. Then, the asphaltene-containing nanoparticles were separated via centrifugation at 10000 rpm for 15 min. To find an acceptable centrifugation speed for the nanoparticle removal from different synthetic oils, several references were studied.[76,80,81] The asphaltene concentration in the supernatant liquids was analyzed with a Dynamica DB20-Spectrophotometer on the quartz cuvette, and toluene was used as the blank.[82] A linear calibration curve of UV–Vis absorbance at a wavelength of 300 nm versus the asphaltene concentration was obtained using standard asphaltene–toluene solutions with known concentrations. The wavelength scan for determining the λ_{max} of asphaltene used in this study and the standard curve, along with the obtaining method, can be seen in Section S2 in the Supporting Information. After that, the absorbance of the supernatant fluid was measured and converted to concentration using the calibration curve.

The adsorption capacity of asphaltene (mg/g) on the PBMA and BMA nanoparticles was calculated employing the mass balance in eq 3.

$$Q = \frac{V(C_0 - C_e)}{m} \tag{3}$$

where Q is the adsorption capacity (mg/g), C_0 is the initial concentration of asphaltene (mg/L), C_e is the equilibrium concentration of asphaltene (mg/L), V is the volume of the synthetic oil (L), and m is the mass of the adsorbent (g).

For measuring the adsorption efficiency (%) of two different nanoparticles toward asphaltene adsorption, eq 4 was utilized.

$$\text{adsorption efficiency (\%)} = \frac{(C_0 - C_e)}{C_0} \times 100 \tag{4}$$

where C_0 is the initial concentration of asphaltene (mg/L), and C_e is the equilibrium concentration of asphaltene (mg/L).

To investigate the asphaltene adsorption capacity of these nanoparticles in different initial concentrations of asphaltenes, the adsorption experiments were conducted for four synthetic oils containing 500, 1000, 3000, and 5000 ppm asphaltene in a specific concentration of carboxylate-alumoxane nanoparticles resulting from the adsorption capacity experiments in various concentrations of nanoparticles. Marczewski and Szymula[83] reported that 3000 ppm asphaltene concentration is the critical micelle concentration (CMC) of asphaltene molecules. Thus, 500 and 1000 ppm asphaltene concentrations are lower than the CMC of asphaltene. On the other hand, 5000 ppm asphaltene concentration is higher than the CMC of asphaltene. Therefore, by selecting these concentrations of asphaltene for adsorption experiments, the adsorption capacity of PBMA and BMA nanoparticles can be investigated in the CMC of asphaltene, lower than the CMC of asphaltene and higher than the CMC of asphaltene. For obtaining the adsorption capacity values, eq 3 was also exerted, and m was constant for these four samples.

4.5. Indirect Technique for Onset Point Detection. For evaluating the asphaltene precipitation onset point and the amount of precipitated asphaltene (%), the indirect technique devised by Tavakkoli et al.[44] was employed. The procedure of this method is illustrated in Figure 17. For conducting this method, various volume ratios of synthetic oil and *n*-heptane

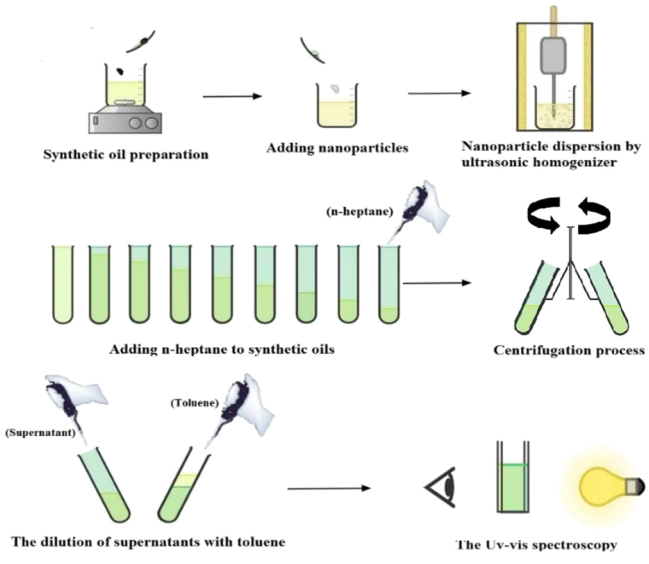

Figure 17. Indirect method schematic used for determining the onset point of asphaltene precipitation.

https://dx.doi.org/10.1021/acsomega.0c01732
ACS Omega 2020, 5, 16149–16164

ranging from 0 to 80% *n*-heptane were produced in sample tubes. To dissolve *n*-heptane in synthetic oil completely, the sample tubes were shaken by hand for a specific amount of time. Then, the sample tubes were allowed to settle for 2 h to obtain the aging time. For the elimination of unstable asphaltenes, the centrifugation of samples was performed by the Universal PIT 320 centrifuge, setting the centrifuge device at the speed of 10,000 rpm for 15 min. The speed applied for the centrifugation of samples is vital to assist in the increment of sediment packing that contributed to the avoidance of asphaltene resuspension in centrifuge tubes (Falcons). To determine the onset of asphaltene precipitation, a Dynamica DB20-Spectrophotometer set at the wavelength of 600 nm was used with a quartz cuvette as a spectrophotometer cell, and the blank was air in all experiments. The reason for the 600 nm wavelength selection is discussed in Section S3 in the Supporting Information. Before using the UV−Vis for determining the onset point, 1 CC of the supernatant of different samples was diluted with toluene, whenever required, based on the synthetic oil concentration to an absorbance value compatible with linearity range of calibration curve. Afterward, the effect of dilution attributed to the absorbance of toluene and *n*-heptane was subtracted from the obtained absorbance for different samples. Then, the curves obtained from the data of absorbance were corrected via the correction of dilution impact (the correction method is discussed in Section S4 in the Supporting Information). The data and curves resulting from this experiment were considered as the reference for the onset point of asphaltene precipitation in the absence of nanoparticles.

In the presence of nanoparticles, a specific mass of different carboxylate-alumoxane nanoparticles, which was consistent with the results of adsorption capacity experiments, was dispersed in synthetic oils having the desired concentration. The dispersion of two nanoparticles in various synthetic oils was performed by an ultrasonic disruptor (UP-400 A) from Ultrasonic Technology Development Co. (UTDC), set at the power of 150 W.[84] For affecting the nanoparticles on the synthetic oils, all samples were left for 2 h, relevant to the adsorption capacity experiments. All subsequent steps were the same as those used for preparing the reference samples. Based on several references,[76,80,81] the centrifugation process set at a speed of 10,000 rpm for 15 min is effective for the nanoparticle removal from samples. To guarantee the repeatability of the experiments, all tests were conducted two times, followed by calculation of an average for each point. According to the indirect technique, the difference in optical properties of various samples will exhibit the onset point of asphaltene precipitation in the absence and presence of carboxylate-alumoxane nanoparticles.

4.6. Determining the Precipitated Asphaltene Amount. The amount of precipitated asphaltene was measured by the optical data resulting from UV−Vis tests applied for detecting the asphaltene precipitation onset point. The fact that the optical properties of various supernatants are different contributed to different absorbance values; the concentration of samples will be calculated by employing the calibration curve obtained from different standard solutions. For the calculation of asphaltene concentration, the standard curve plotted in 600 nm (Figure S6 in the Supporting Information) was employed as it had a greater slope, given the maximum absorbance value along with the satisfactory coefficient of determination, R^2. For calculating the precipitated asphaltene percentage, eq 5 was applied.

$$\text{precipitated asphaltene amount (\%)} = \frac{C_i - C_f}{C_i} \times 100 \quad (5)$$

()where C_i is the initial concentration of asphaltene (mg/L), and C_f is the final concentration of asphaltene (mg/L) in supernatant liquid. It should also be mentioned that the concentrations resulting from the standard curve should be modified before calculating the precipitated asphaltene amount because of the dilution impact (Section S4 in the Supporting Information).

■ ASSOCIATED CONTENT

Supporting Information

The Supporting Information is available free of charge at https://pubs.acs.org/doi/10.1021/acsomega.0c01732.

Asphaltene extraction, identifying the λ_{max} of asphaltene molecules and calibration curve for adsorption experiments, identifying a suitable wavelength for performing the experiments related to determining the onset point of asphaltene precipitation, and dilution impact correction (PDF)

■ AUTHOR INFORMATION

Corresponding Authors

Masoud Riazi − *Enhanced Oil Recovery (EOR) Research Center, IOR/EOR Research Institute, Shiraz University, 7194684636 Shiraz, Iran;* orcid.org/0000-0003-0572-1766; Email: mriazi@shirazu.ac.ir

Farid B. Cortés − *Grupo de Investigación en Fenómenos de Superficie Michael Polanyi, Facultad de Minas, Universidad Nacional de Colombia Sede Medellín, 050034, Colombia;* orcid.org/0000-0003-1207-3859; Email: fbcortes@unal.edu.co

Authors

Saman Bagherpour − *Enhanced Oil Recovery (EOR) Research Center, IOR/EOR Research Institute, Shiraz University, 7194684636 Shiraz, Iran; Separation Processes & Nanotechnology Lab, Faculty of Caspian, College of Engineering, University of Tehran, 1417466191 Tehran, Iran;* orcid.org/0000-0001-6131-9654

Mohsen Riazi − *Enhanced Oil Recovery (EOR) Research Center, IOR/EOR Research Institute, Shiraz University, 7194684636 Shiraz, Iran; Department of Petroleum Engineering, Shahid Bahonar University of Kerman, 7616914111 Kerman, Iran*

Seyed Hamed Mousavi − *Separation Processes & Nanotechnology Lab, Faculty of Caspian, College of Engineering, University of Tehran, 1417466191 Tehran, Iran*

Complete contact information is available at: https://pubs.acs.org/10.1021/acsomega.0c01732

Notes

The authors declare no competing financial interest.

■ ACKNOWLEDGMENTS

The authors acknowledge the Enhanced Oil Recovery (EOR) Research Center, IOR/EOR Research Institute, Shiraz University, for the logistical and financial support. Also, the

authors are grateful to Dr. Yousef Kazemzadeh for his valuable advice.

REFERENCES

(1) Balabin, R. M.; Syunyaev, R. Z.; Schmid, T.; Stadler, J.; Lomakina, E. I.; Zenobi, R. Asphaltene adsorption onto an iron surface: combined near-infrared (NIR), Raman, and AFM study of the kinetics, thermodynamics, and layer structure. *Energy Fuels* **2011**, *25*, 189−196.

(2) Nassar, N. N.; Montoya, T.; Franco, C. A.; Cortés, F. B.; Pereira-Almao, P. A new model for describing the adsorption of asphaltenes on porous media at a high pressure and temperature under flow conditions. *Energy Fuels* **2015**, *29*, 4210−4221.

(3) Schuler, B.; Meyer, G.; Peña, D.; Mullins, O. C.; Gross, L. Unraveling the Molecular Structures of Asphaltenes by Atomic Force Microscopy. *J. Am. Chem. Soc.* **2015**, *137*, 9870−9876.

(4) Lin, Y.-J.; He, P.; Tavakkoli, M.; Mathew, N. T.; Fatt, Y. Y.; Chai, J. C.; Goharzadeh, A.; Vargas, F. M.; Biswal, S. L. Examining asphaltene solubility on deposition in model porous media. *Langmuir* **2016**, *32*, 8729−8734.

(5) Ancheyta, J.; Trejo, F.; Rana, M. S. *Asphaltenes: chemical transformation during hydroprocessing of heavy oils*; 1st ed.; CRC Press: Boca Raton, 2010; pp 1−86, DOI: 10.1201/9781420066319.

(6) Kazemzadeh, Y.; Parsaei, R.; Riazi, M. Experimental study of asphaltene precipitation prediction during gas injection to oil reservoirs by interfacial tension measurement. *Colloids Surf., A* **2015**, *466*, 138−146.

(7) Joonaki, E.; Hassanpouryouzband, A.; Burgass, R.; Hase, A.; Tohidi, B. Effects of Waxes and the Related Chemicals on Asphaltene Aggregation and Deposition Phenomena: Experimental and Modeling Studies. *ACS Omega* **2020**, *5*, 7124−7134.

(8) Shahebrahimi, Y.; Fazlali, A.; Motamedi, H.; Kord, S.; Mohammadi, A. H. Effect of Various Isolated Microbial Consortiums on the Biodegradation Process of Precipitated Asphaltenes from Crude Oil. *ACS Omega* **2020**, *5*, 3131−3143.

(9) Bera, A.; Agarwal, J.; Shah, M.; Shah, S.; Vij, R. K. Recent advances in ionic liquids as alternative to surfactants/chemicals for application in upstream oil industry. *J. Ind. Eng. Chem.* **2020**, *82*, 17−30.

(10) Mohammadi, M.; Akbari, M.; Fakhroueian, Z.; Bahramian, A.; Azin, R.; Arya, S. Inhibition of Asphaltene Precipitation by TiO_2, SiO_2, and ZrO_2 Nanofluids. *Energy Fuels* **2011**, *25*, 3150−3156.

(11) Hou, B.; Jia, R.; Fu, M.; Wang, Y.; Bai, Y.; Huang, Y. Wettability alteration of an oil-wet sandstone surface by synergistic adsorption/desorption of cationic/nonionic surfactant mixtures. *Energy Fuels* **2018**, *32*, 12462−12468.

(12) Hou, B.; Jia, R.; Fu, M.; Huang, Y.; Wang, Y. Mechanism of Wettability Alteration of an Oil-Wet Sandstone Surface by a Novel Cationic Gemini Surfactant. *Energy Fuels* **2019**, *33*, 4062−4069.

(13) Hou, B.; Jia, R.; Fu, M.; Li, L.; Xu, T.; Jiang, C. Mechanism of synergistically changing wettability of an oil-wet sandstone surface by a novel nano-active fluid. *Energy Fuels* **2020**, DOI: 10.1021/acs.energyfuels.0c00521.

(14) Moncayo-Riascos, I.; Taborda, E.; Hoyos, B. A.; Franco, C. A.; Cortés, F. B. Theoretical-experimental evaluation of rheological behavior of asphaltene solutions in toluene and p-xylene: Effect of the additional methyl group. *J. Mol. Liq.* **2020**, *303*, 112664.

(15) Ismail, I.; Kazemzadeh, Y.; Sharifi, M.; Riazi, M.; Malayeri, M. R.; Cortés, F. Formation and stability of W/O emulsions in presence of asphaltene at reservoir thermodynamic conditions. *J. Mol. Liq.* **2020**, *299*, 112125.

(16) Medina, O. E.; Gallego, J.; Rodríguez, E.; Franco, C. A.; Cortés, F. B. Effect of pressure on the oxidation kinetics of Asphaltenes. *Energy Fuels* **2019**, *33*, 10734−10744.

(17) Medina, O. E.; Gallego, J.; Restrepo, L. G.; Cortés, F. B.; Franco, C. A. Influence of the Ce^{4+}/Ce^{3+} Redox-couple on the cyclic regeneration for adsorptive and catalytic performance of NiO-PdO/$CeO_{2\pm\delta}$ nanoparticles for n-C_7 asphaltene steam gasification. *Nanomaterials* **2019**, *9*, 734.

(18) Rashid, Z.; Wilfred, C. D.; Iyyaswami, R.; Appusamy, A.; Thanabalan, M. Investigating the solubility of Petroleum Asphaltene in ionic liquids and their interaction using COSMO-RS. *J. Ind. Eng. Chem.* **2019**, *79*, 194−203.

(19) Hu, Y.-F.; Guo, T.-M. Effect of the structures of ionic liquids and alkylbenzene-derived amphiphiles on the inhibition of asphaltene precipitation from CO_2-injected reservoir oils. *Langmuir* **2005**, *21*, 8168−8174.

(20) León, O.; Contreras, E.; Rogel, E.; Dambakli, G.; Espidel, J.; Acevedo, S. The influence of the adsorption of amphiphiles and resins in controlling asphaltene flocculation. *Energy Fuels* **2001**, *15*, 1028−1032.

(21) Dehaghani, A. H. S.; Badizad, M. H. Inhibiting asphaltene precipitation from Iranian crude oil using various dispersants: experimental investigation through viscometry and thermodynamic modelling. *Fluid Phase Equilib.* **2017**, *442*, 104−118.

(22) Kazemzadeh, Y.; Malayeri, M. R.; Riazi, M.; Parsaei, R. Impact of Fe_3O_4 nanoparticles on asphaltene precipitation during CO_2 injection. *J. Nat. Gas Sci. Eng.* **2015**, *22*, 227−234.

(23) Franco, C. A.; Nassar, N. N.; Ruiz, M. A.; Pereira-Almao, P.; Cortés, F. B. Nanoparticles for inhibition of asphaltenes damage: adsorption study and displacement test on porous media. *Energy Fuels* **2013**, *27*, 2899−2907.

(24) Franco, C.; Patiño, E.; Benjumea, P.; Ruiz, M. A.; Cortés, F. B. Kinetic and thermodynamic equilibrium of asphaltenes sorption onto nanoparticles of nickel oxide supported on nanoparticulated alumina. *Fuel* **2013**, *105*, 408−414.

(25) Li, X.; Guo, Y.; Sun, Q.; Lan, W.; Guo, X. Effect of Nanoparticles on Asphaltene Aggregation in a Microsized Pore. *Ind. Eng. Chem. Res.* **2018**, *57*, 9009−9017.

(26) Derikvand, Z.; Rezaei, A.; Parsaei, R.; Riazi, M.; Torabi, F. A mechanistic experimental study on the combined effect of Mg^{2+}, Ca^{2+}, and SO_4^{2-} ions and a cationic surfactant in improving the surface properties of oil/water/rock system. *Colloids Surf., A* **2020**, *587*, 124327.

(27) Parsaei, R.; Kazemzadeh, Y.; Riazi, M. Study of Asphaltene Precipitation during CO_2 Injection into Oil Reservoirs in the Presence of Iron Oxide Nanoparticles by Interfacial Tension and Bond Number Measurements. *ACS Omega* **2020**, 7877.

(28) Medina, O. E.; Gallego, J.; Olmos, C. M.; Chen, X.; Cortés, F. B.; Franco, C. A. Effect of Multifunctional Nanocatalysts on n-C_7 Asphaltene Adsorption and Subsequent Oxidation under High-Pressure Conditions. *Energy Fuels* **2020**, 6261.

(29) Medina, O. E.; Gallego, J.; Arias-Madrid, D.; Cortés, F. B.; Franco, C. A. Optimization of the load of transition metal oxides (Fe_2O_3, Co_3O_4, NiO and/or PdO) onto CeO_2 nanoparticles in catalytic steam decomposition of n-C_7 asphaltenes at low temperatures. *Nanomaterials* **2019**, *9*, 401.

(30) Nassar, N. N.; Betancur, S.; Acevedo, S.; Franco, C. A.; Cortés, F. B. Development of a population balance model to describe the influence of shear and nanoparticles on the aggregation and fragmentation of asphaltene aggregates. *Ind. Eng. Chem. Res.* **2015**, *54*, 8201−8211.

(31) Franco, C. A.; Nassar, N. N.; Montoya, T.; Ruíz, M. A.; Cortés, F. B. Influence of asphaltene aggregation on the adsorption and catalytic behavior of nanoparticles. *Energy Fuels* **2015**, *29*, 1610−1621.

(32) Nassar, N. N.; Hassan, A.; Pereira-Almao, P. Effect of surface acidity and basicity of aluminas on asphaltene adsorption and oxidation. *J. Colloid Interface Sci.* **2011**, *360*, 233−238.

(33) Lu, T.; Li, Z.; Fan, W.; Zhang, X.; Lv, Q. Nanoparticles for inhibition of asphaltenes deposition during CO_2 flooding. *Ind. Eng. Chem. Res.* **2016**, *55*, 6723−6733.

(34) Cortés, F. B.; Mejía, J. M.; Ruiz, M. A.; Benjumea, P.; Riffel, D. B. Sorption of asphaltenes onto nanoparticles of nickel oxide supported on nanoparticulated silica gel. *Energy Fuels* **2012**, *26*, 1725−1730.

(35) Zabala, R.; Mora, E.; Botero, O.; Cespedes, C.; Guarin, L.; Franco, C.; Cortes, F.; Patino, J.; Ospina, N. Nano-technology for asphaltenes inhibition in Cupiagua South Wells. In *IPTC 2014:*

https://dx.doi.org/10.1021/acsomega.0c01732
ACS Omega 2020, 5, 16149−16164

International Petroleum Technology Conference; European Association of Geoscientists & Engineers: 2014, DOI: 10.3997/2214-4609-pdb.395.IPTC-17344-MS.
(36) Derakhshan, A. A.; Rajabi, L. Review on applications of carboxylate−alumoxane nanostructures. *Powder Technol.* **2012**, *226*, 117−129.
(37) Kareiva, A.; Harlan, C. J.; MacQueen, D. B.; Cook, R. L.; Barron, A. R. Carboxylate-Substituted Alumoxanes as Processable Precursors to Transition Metal− Aluminum and Lanthanide−Aluminum Mixed-Metal Oxides: Atomic Scale Mixing via a New Transmetalation Reaction. *Chem. Mater.* **1996**, *8*, 2331−2340.
(38) Obrey, S. J.; Barron, A. R. A Chemically Functionalized Carboxylate− Alumoxane Nanoparticle Support for Olefin Polymerization Catalysts. *Macromolecules* **2002**, *35*, 1499−1503.
(39) Mistry, A. S.; Mikos, A. G.; Jansen, J. A. Degradation and biocompatibility of a poly(propylene fumarate)-based/alumoxane nanocomposite for bone tissue engineering. *J. Biomed. Mater. Res., Part A* **2007**, *83A*, 940−953.
(40) Fey, G. T.-K.; Chen, J.-G.; Prem Kumar, T. Carboxylate-alumoxanes as precursors for alumina coatings to enhance the cyclability of $LiCoO_2$. *J. Power Sources* **2005**, *146*, 250−253.
(41) Baker, B. R.; Pearson, R. M. Water content of pseudoboehmite: A new model for its structure. *J. Catal.* **1974**, *33*, 265−278.
(42) Tettenhorst, R.; Hofmann, D. A. Crystal chemistry of boehmite. *Clays Clay Miner.* **1980**, *28*, 373−380.
(43) Pahlavan, F.; Hung, A. M.; Zadshir, M.; Hosseinnezhad, S.; Fini, E. H. Alteration of π-Electron Distribution To Induce Deagglomeration in Oxidized Polar Aromatics and Asphaltenes in an Aged Asphalt Binder. *ACS Sustainable Chem. Eng.* **2018**, *6*, 6554−6569.
(44) Tavakkoli, M.; Grimes, M. R.; Liu, X.; Garcia, C. K.; Correa, S. C.; Cox, Q. J.; Vargas, F. M. Indirect method: a novel technique for experimental determination of asphaltene precipitation. *Energy Fuels* **2015**, *29*, 2890−2900.
(45) Shojaati, F.; Riazi, M.; Mousavi, S. H.; Derikvand, Z. Experimental investigation of the inhibitory behavior of metal oxides nanoparticles on asphaltene precipitation. *Colloids Surf., A* **2017**, *531*, 99−110.
(46) Shojaati, F.; Mousavi, S. H.; Riazi, M.; Torabi, F.; Osat, M. Investigating the effect of salinity on the behavior of asphaltene precipitation in the presence of emulsified water. *Ind. Eng. Chem. Res.* **2017**, *56*, 14362−14368.
(47) Vogelson, C. T.; Barron, A. R. Particle size control and dependence on solution pH of carboxylate−alumoxane nanoparticles. *J. Non-Cryst. Solids* **2001**, *290*, 216−223.
(48) Sifontes, Á. B.; Gutierrez, B.; Mónaco, A.; Yanez, A.; Díaz, Y.; Méndez, F. J.; Llovera, L.; Cañizales, E.; Brito, J. L. Preparation of functionalized porous nano-γ-Al_2O_3 powders employing colophony extract. *Biotechnol. Rep.* **2014**, *4*, 21−29.
(49) Xu, D.; Jiang, H.; Li, M.; Hai, O.; Zhang, Y. Synthesis and characterization of Y_2O_3 doped Na−β''-Al_2O_3 solid electrolyte by double zeta process. *Ceram. Int.* **2015**, *41*, 5355−5361.
(50) Bagherpour, S.; Rashidi, A.; Mousavi, S. H.; Izadi, N.; Hamidpour, E. Experimental investigation of carboxylate-alumoxane nanoparticles for the enhanced oil recovery performance. *Colloids Surf., A* **2019**, *563*, 37−49.
(51) Bakhtiari, N.; Azizian, S. Adsorption of copper ion from aqueous solution by nanoporous MOF-5: a kinetic and equilibrium study. *J. Mol. Liq.* **2015**, *206*, 114−118.
(52) Groen, J. C.; Peffer, L. A. A.; Pérez-Ramírez, J. Pore size determination in modified micro- and mesoporous materials. Pitfalls and limitations in gas adsorption data analysis. *Microporous Mesoporous Mater.* **2003**, *60*, 1−17.
(53) Cao, J.; Yang, Z.-h.; Xiong, W.-p.; Zhou, Y.-y.; Peng, Y.-r.; Li, X.; Zhou, C.-y.; Xu, R.; Zhang, Y.-r. One-step synthesis of Co-doped UiO-66 nanoparticle with enhanced removal efficiency of tetracycline: Simultaneous adsorption and photocatalysis. *Chem. Eng. J.* **2018**, *353*, 126−137.
(54) Chen, F.; Zhao, E.; Kim, T.; Wang, J.; Hableel, G.; Reardon, P. J. T.; Ananthakrishna, S. J.; Wang, T.; Arconada-Alvarez, S.; Knowles, J. C.; Jokerst, J. V. Organosilica Nanoparticles with an Intrinsic Secondary Amine: An Efficient and Reusable Adsorbent for Dyes. *ACS Appl. Mater. Interfaces* **2017**, *9*, 15566−15576.
(55) Huynh, J.; Palacio, R.; Safizadeh, F.; Lefèvre, G.; Descostes, M.; Eloy, L.; Guignard, N.; Rousseau, J.; Royer, S.; Tertre, E.; Batonneau-Gener, I. Adsorption of Uranium over NH_2-Functionalized Ordered Silica in Aqueous Solutions. *ACS Appl. Mater. Interfaces* **2017**, *9*, 15672−15684.
(56) Guzmán, J. D.; Betancur, S.; Carrasco-Marín, F.; Franco, C. A.; Nassar, N. N.; Cortés, F. B. Importance of the adsorption method used for obtaining the nanoparticle dosage for asphaltene-related treatments. *Energy Fuels* **2016**, *30*, 2052−2059.
(57) Feng, Y.; Gong, J.-L.; Zeng, G.-M.; Niu, Q.-Y.; Zhang, H.-Y.; Niu, C.-G.; Deng, J.-H.; Yan, M. Adsorption of Cd (II) and Zn (II) from aqueous solutions using magnetic hydroxyapatite nanoparticles as adsorbents. *Chem. Eng. J.* **2010**, *162*, 487−494.
(58) Hao, Y.-M.; Man, C.; Hu, Z.-B. Effective removal of Cu (II) ions from aqueous solution by amino-functionalized magnetic nanoparticles. *J. Hazard. Mater.* **2010**, *184*, 392−399.
(59) Bagwe, R. P.; Hilliard, L. R.; Tan, W. Surface Modification of Silica Nanoparticles to Reduce Aggregation and Nonspecific Binding. *Langmuir* **2006**, *22*, 4357−4362.
(60) Hou, B.; Jia, R.; Fu, M.; Wang, Y.; Jiang, C.; Yang, B.; Huang, Y. Wettability alteration of oil-wet carbonate surface induced by self-dispersing silica nanoparticles: Mechanism and monovalent metal ion's effect. *J. Mol. Liq.* **2019**, *294*, 111601.
(61) Ivanova, A. A.; Phan, C.; Barifcani, A.; Iglauer, S.; Cheremisin, A. N. Effect of Nanoparticles on Viscosity and Interfacial Tension of Aqueous Surfactant Solutions at High Salinity and High Temperature. *J. Surfactants Deterg.* **2019**, 327.
(62) Rezaei, A.; Riazi, M.; Escrochi, M.; Elhaei, R. Integrating surfactant, alkali and nano-fluid flooding for enhanced oil recovery: A mechanistic experimental study of novel chemical combinations. *J. Mol. Liq.* **2020**, 113106.
(63) Betancur, S.; Carmona, J. C.; Nassar, N. N.; Franco, C. A.; Cortés, F. B. Role of particle size and surface acidity of silica gel nanoparticles in inhibition of formation damage by asphaltene in oil reservoirs. *Ind. Eng. Chem. Res.* **2016**, *55*, 6122−6132.
(64) Yudin, I. K.; Nikolaenko, G. L.; Gorodetskii, E. E.; Kosov, V. I.; Melikyan, V. R.; Markhashov, E. L.; Frot, D.; Briolant, Y. Mechanisms of asphaltene aggregation in toluene−heptane mixtures. *J. Pet. Sci. Eng.* **1998**, *20*, 297−301.
(65) Kim, I.; Taghavy, A.; DiCarlo, D.; Huh, C. Aggregation of silica nanoparticles and its impact on particle mobility under high-salinity conditions. *J. Pet. Sci. Eng.* **2015**, *133*, 376−383.
(66) Franco, C. A.; Lozano, M. M.; Acevedo, S.; Nassar, N. N.; Cortés, F. B. Effects of resin I on asphaltene adsorption onto nanoparticles: a novel method for obtaining asphaltenes/resin isotherms. *Energy Fuels* **2016**, *30*, 264−272.
(67) Langmuir, I. The adsorption of gases on plane surfaces of glass, mica and platinum. *J. Am. Chem. Soc.* **1918**, *40*, 1361−1403.
(68) Ng, C.; Losso, J. N.; Marshall, W. E.; Rao, R. M. Freundlich adsorption isotherms of agricultural by-product-based powdered activated carbons in a geosmin−water system. *Bioresour. Technol.* **2002**, *85*, 131−135.
(69) Nassar, N. N.; Hassan, A.; Pereira-Almao, P. Metal oxide nanoparticles for asphaltene adsorption and oxidation. *Energy Fuels* **2011**, *25*, 1017−1023.
(70) Franco, C. A.; Montoya, T.; Nassar, N. N.; Pereira-Almao, P.; Cortés, F. B. Adsorption and subsequent oxidation of colombian asphaltenes onto nickel and/or palladium oxide supported on fumed silica nanoparticles. *Energy Fuels* **2013**, *27*, 7336−7347.
(71) Ben-Ali, S.; Jaouali, I.; Souissi-Najar, S.; Ouederni, A. Characterization and adsorption capacity of raw pomegranate peel biosorbent for copper removal. *J. Cleaner Prod.* **2017**, *142*, 3809−3821.

(72) Hosseinpour, N.; Khodadadi, A. A.; Bahramian, A.; Mortazavi, Y. Asphaltene adsorption onto acidic/basic metal oxide nanoparticles toward in situ upgrading of reservoir oils by nanotechnology. *Langmuir* **2013**, *29*, 14135−14146.
(73) Ezeonyeka, N. L.; Hemmati-Sarapardeh, A.; Husein, M. M. Asphaltenes Adsorption onto Metal Oxide Nanoparticles: A Critical Evaluation of Measurement Techniques. *Energy Fuels* **2018**, *32*, 2213−2223.
(74) Sun, J.; Liu, R.; Tang, J.; Zhang, Z.; Zhou, X.; Liu, J. Controlled Assembly of Gold Nanostructures on a Solid Substrate via Imidazole Directed Hydrogen Bonding for High Performance Surface Enhance Raman Scattering Sensing of Hypochlorous Acid. *ACS Appl. Mater. Interfaces* **2015**, *7*, 16730−16737.
(75) Yamasaki, T. Structure and Lewis acid sites in alumoxane compounds. *Catal. Today* **1995**, *23*, 425−429.
(76) Nassar, N. N. Asphaltene Adsorption onto Alumina Nanoparticles: Kinetics and Thermodynamic Studies. *Energy Fuels* **2010**, *24*, 4116−4122.
(77) Zhang, K.; Hu, Y.; Wang, L.; Monteiro, M. J.; Jia, Z. Pyrene-Functionalized PTMA by NRC for Greater $\pi-\pi$ Stacking with rGO and Enhanced Electrochemical Properties. *ACS Appl. Mater. Interfaces* **2017**, *9*, 34900−34908.
(78) Corredor-Rojas, L. M.; Hemmati-Sarapardeh, A.; Husein, M. M.; Dong, M.; Maini, B. B. Rheological Behavior of Surface Modified Silica Nanoparticles Dispersed in Partially Hydrolyzed Polyacrylamide and Xanthan Gum Solutions: Experimental Measurements, Mechanistic Understanding, and Model Development. *Energy Fuels* **2018**, *32*, 10628−10638.
(79) Callender, R. L.; Harlan, C. J.; Shapiro, N. M.; Jones, C. D.; Callahan, D. L.; Wiesner, M. R.; MacQueen, D. B.; Cook, R.; Barron, A. R. Aqueous Synthesis of Water-Soluble Alumoxanes: Environmentally Benign Precursors to Alumina and Aluminum-Based Ceramics. *Chem. Mater.* **1997**, *9*, 2418−2433.
(80) Nassar, N. N.; Hassan, A.; Pereira-Almao, P. Application of Nanotechnology for Heavy Oil Upgrading: Catalytic Steam Gasification/Cracking of Asphaltenes. *Energy Fuels* **2011**, *25*, 1566−1570.
(81) Alboudwarej, H.; Pole, D.; Svrcek, W. Y.; Yarranton, H. W. Adsorption of Asphaltenes on Metals. *Ind. Eng. Chem. Res.* **2005**, *44*, 5585−5592.
(82) Franco, C. A.; Nassar, N. N.; Cortés, F. B. Removal of oil from oil-in-saltwater emulsions by adsorption onto nano-alumina functionalized with petroleum vacuum residue. *J. Colloid Interface Sci.* **2014**, *433*, 58−67.
(83) Marczewski, A. W.; Szymula, M. Adsorption of asphaltenes from toluene on mineral surface. *Colloids Surf., A* **2002**, *208*, 259−266.
(84) Rezaei, A.; Abdollahi, H.; Derikvand, Z.; Hemmati-Sarapardeh, A.; Mosavi, A.; Nabipour, N. Insights into the Effects of Pore Size Distribution on the Flowing Behavior of Carbonate Rocks: Linking a Nano-Based Enhanced Oil Recovery Method to Rock Typing. *Nanomaterials* **2020**, *10*, 972.

https://dx.doi.org/10.1021/acsomega.0c01732
ACS Omega 2020, 5, 16149−16164